BOLD MRI TO EVALUATE LIVER FUNCTION

EVALUATION OF LIVER FUNCTION IN HEALTHY SUBJECTS AND LIVER DISEASE PATIENTS USING BOLD MRI

By

ALYAA H. ELZIBAK, HON.B.SC.

A Thesis

Submitted to the School of Graduate Studies

in Partial Fulfilment of the Requirements

for the Degree

Master of Science

McMaster University

MASTER OF SCEINCE (2008) McMaster University

(Medical Physics and Applied Radiation Sciences) Hamilton, Ontario

TITLE: Evaluation of Liver Function in Healthy Subjects and Liver Disease Patients Using BOLD MRI

AUTHOR: Alyaa H. Elzibak, Hon.B.Sc.(McMaster University)

SUPERVISOR: Michael D. Noseworthy, Ph.D.

NUMBER OF PAGES: xvii, 88

Abstract

The liver is a multi-function organ that plays important roles in nutrient metabolism, biochemical transformations and blood detoxification. The purpose of the current work was to optimize Blood Oxygen Level Dependent (BOLD) liver functional MR imaging and analysis to allow the distinction between healthy volunteers and subjects with chronic liver disorders known to lead to fibrosis and reduced liver function (in this case, Hepatitis-C).

Liver BOLD signal can be modulated by breathing 100% O_2 or through intake of a meal. Previous results using these stimuli have been inconclusive when comparing healthy and diseased livers. In addition, liver BOLD analysis has been traditionally carried out using general linear models (GLM). Since the liver has a dual blood supply (portal and arterial derived), its resultant haemodynamic response is complex. This makes it too difficult to employ GLM approaches, as they require the prediction and modeling of a response function. We chose a model-free, or data-driven approach, called principle component analysis (PCA) to analyze liver data.

Initial optimization was done by determining the time of maximal hepatic portal vein (HPV) blood flow following ingestion of a controlled meal (235 mL of Ensure Plus®). Statistically significant increases in HPV flow resulted at all measurement intervals, with the maximal postprandial change (71% increase in comparison to the baseline flow) at thirty minutes after ingestion.

Implementing acquisition and analysis optimizations with our dual liver challenge model (hyperoxia cycling in pre- and postprandial states), the PCA

approach was able to detect all of the diseased livers (n=6), while missing four of the healthy subjects (n=11). The GLM technique, on the other hand, did not detect two of the patients and two of the healthy subjects. Thus, if this liver challenge is to be used as a screening tool, a model-free data analysis approach is suggested as more appropriate since it minimizes the chances of reporting false-negative results (based on this preliminary cohort). Although more false positives were detected with this method, it is of less concern seeing as these inaccuracies can be screened using simple blood tests. Promising results were obtained in this project, however, further studies using data-driven approaches such as partial least squares (PLS) are needed.

Acknowledgements

I would like to express my sincere appreciation to everyone who provided encouragement and direction throughout my graduate years.

First of all, I want to thank my supervisor, Dr. Michael Noseworthy, for his guidance and kind support. The training that you provided during the past two years will definitely ease my transition along the academic career ladder. I would also like to thank my supervisory committee members: Dr. Colm Boylan, Dr. Fiona McNeill and Dr. Gervais Tougas. Patient recruitment was an important part of this project and this would not have been possible without your help Dr. Boylan. Thank you very much. I am especially grateful to Dr. Jeff Fortuna for his time and insightful discussions. You were always willing to patiently answer the many questions that I had about principle component analysis.

Acquiring MR images was a must for this project. Not only did the MR technologists make this possible, they also ensured that each imaging session ran smoothly. A special thank you to Cheryl Constant, Janet Burr and Jay Neadles.

Besides those who contributed to the actual project, there were many individuals whose input came in the form of emotional support. I would first like to thank my colleagues at the Imaging Research Center. You were constantly sharing your own experiences and encouraging me when I thought I reached a dead end. I would also like to extend my appreciation to my family for being there for me. Father and mother, I am truly grateful for all your support. To my fiancé, siblings and extended family, thank you for the encouragement that you provided. Last, but definitely not least, I want to sincerely thank my friends and mentors for their inspirational words of wisdom.

Table of Contents

Abstract iii

Acknowledgements v

List of Figures ix

List of Tables xii

List of Notations and Abbreviations xv

Chapter 1 The Liver **1**

1.1 Anatomy 1

1.2 Physiology 3

1.3 Diseases 3

1.4 Evaluation of Liver Function 4

Chapter 2 BOLD MRI **9**

2.1 Theory 9

2.2 Hypothesis Driven Analysis of the BOLD Time-series 12

2.3 Data Driven Analysis of the BOLD Time-series 16

2.4 Applying the BOLD Effect to the Evaluation of Liver Function 18

2.5 Literature Review 19

Chapter 3 Problem Definition and Hypothesis **22**

3.1 Problem Definition 22

3.2 Hypothesis Statement and Proposed Solution 23

Chapter 4 Materials and Methods **26**

4.1 MR Scanner 26

4.2 Blood Flow 26

4.2.1 Accessories 27

4.2.2 Protocol 27

4.2.3 Subjects 28

4.2.4 Data Analysis 28

4.3 BOLD Experiments 29

4.3.1 Accessories 29

4.3.2 Protocol 30

4.3.3 Liver Challenge Procedure 31

4.3.4 Subjects 33

4.3.5 Data Analysis 35

Chapter 5 Results **43**

5.1 Blood Flow 43

5.1.1 Baseline Hepatic Portal Vein flow 43

5.1.2 Operator's Error 43

5.1.3 Variation within Subject 44

5.1.4 Effect of Intake of Ensure Plus® 44

5.2 BOLD Experiments 46

5.2.1 Hypothesis Driven Analysis (GLM) 46

5.2.2 Data Driven Analysis (PCA) 54

Chapter 6 Discussion **61**

6.1 Blood Flow 61

6.2 BOLD 63

Appendix A Matlab Code to Create a Registered BOLD Data Set **83**

Appendix B Matlab Code to Calculate the % of Liver that is Responsive **85**

Appendix C Matlab Code to Perform a T-test on the Extracted Liver Data **87**

List of Figures

2.1 Under basal conditions, there is a certain ratio of oxyHB to deoxyHB in a blood vessel. Physiological changes alter this ratio, thereby affecting the BOLD signal. 11

2.2 A sample block design and the idealized waveform. 13

2.3 Collected BOLD time-series and the predicted response for a case where the time-varying signal fits the model (2.3(a)) and one where it is not a good fit (2.3(b)). 14

4.1 Model 1: a timing diagram of the gases that were cycled through to induce changes in liver oxygenation. 32

4.2 Model 2: a timing diagram of the gases that were cycled through to induce changes in liver oxygenation. 32

4.3 Timing diagram for the entire BOLD imaging procedure including both hyperoxia sessions and meal intake. 33

4.4 The motion tracking program: by choosing a liver region to be tracked (area enclosed by the yellow box in the image), the algorithm calculated the position of the template that maximized the correlation coefficient. 37

4.5 The applied stimulus (top) for set-up 1 along with the idealized predicted response (bottom). 38

4.6 The applied stimulus (top) for set-up 2 along with the idealized predicted response (bottom). 38

4.7 The selected segments (shown in grey) for the data driven analysis for the first model (top) and the the second model (bottom). 41

5.1 Blood flow in the portal vein before and after the intake of a can of Ensure Plus®. Results are shown as a mean and standard deviation. Significant changes from baseline measurements were noted at all intervals (P<0.004). 45

5.2 Two time-series representing a negative responder (5.2(a)) and a positive responder (5.2(b)) obtained using gas cycling model 1 (i.e. 3 phases of 3 minutes 100% O_2 separated by 5 minutes of normoxia). 47

5.3 The response maps for the pre and post intake sessions for one healthy subject and one patient with chronic liver disease. A hypothesis driven analysis method was used to obtain the response maps, here using gas cycling model 1. 50

5.4 A sample time-series from one of the subjects with the modified set-up. 52

5.5 The response maps for the pre and post intake sessions for one healthy subject and one patient with chronic liver disease. A hypothesis driven analysis was used to obtain the response maps, here using gas cycling model 2. 53

5.6 The response maps for the pre and post intake sessions for one healthy subject and one patient with liver disorder. Data driven analysis was used to obtain the response maps and gas cycling model 1. 56

5.7 The response maps for the pre and post intake sessions for one healthy subject and one patient with liver disorder. Data driven analysis was used to obtain the response maps and with gas cycling model 2. 58

5.8 The response maps for the pre and post intake sessions for one healthy subject where the second session began either immediately following meal intake (5.8(a)) or 30 minutes postprandial (5.8(b)). 60

6.1 The response maps for the pre and post intake sessions for one healthy subject using a negative ideal wave response(6.1(b)) and a positive ideal wave response (6.1(a)) in the hypothesis driven analysis. 71

6.2 Left: Response map using PCA analysis. Center: The time-series of the selected region. Right: Response map using hypothesis driven analysis. Note that PCA is able to identify the responsive region, while the hypothesis driven technique is not. 72

List of Tables

4.1 Diagnoses of the patients that took part in the study. 34

5.1 Percent change in portal vein blood flow 44

5.2 The percent of liver that had BOLD signal change in the pre and postprandial states for the negative responders (1-3), positive responders (4-8) and patients with liver disease (9-11) using gas cycling model 1. 48

5.3 The percentage change in liver response between the pre and postprandial states for healthy subjects (1-8) and those with liver disease (9-11) using response maps from the hypothesis driven analysis and gas cycling model 1. 51

5.4 The percentage of liver that was responsive in the pre and postprandial states for healthy subjects (1-3) and chronic liver disease patients (4-6) using inspired gas cycling model 2. 54

5.5 Percent change in liver response between pre and postprandial states for healthy subjects (1-3) and those with chronic liver disease (4-6) using response maps from the hypothesis driven analysis (i.e. GLM) with gas cycling model 2. 55

5.6 The percentage change in liver response between the pre and postprandial states for healthy subjects (1-8) and those with liver disease (9-11) using response maps from the data driven analysis and with gas cycling model 1. 57

5.7 The percentage change in liver response between pre and postprandial states for healthy subjects (1-3) and those with liver disease (4-6) using response maps from the data driven analysis with gas cycling model 2. 59

5.8 The percentage change in liver response between the pre and postprandial states for one healthy subject where the second session began either immediately following meal intake or 30 minutes postprandial. 59

List of Notations and Abbreviations

ALP	Alkaline phosphatase
ALT	Alanine aminotransferase
AST	Aspartate aminotransferase
AW	Advantage windows
BOLD	Blood oxygen level dependent
CT	Computed Tomography
CV	Control Variable
DeoxyHB	Deoxyhemoglobin
EPI	Echo planar imaging
FDG	Fluorodeoxyglucose
FEAT	FMRI Expert Analysis Tool
FIESTA	Fast Imaging Employing Steady-state Acquisition
fMRI	Functional Magnetic Resonance Imaging
FSL	FMRIB's Software Library
GE	General Electric
GRE	Gradient recalled echo
HPV	Hepatic portal vein
LFT	Liver function test
MRI	Magnetic resonance imaging
MR	Magnetic resonance
MRI	Magnetic resonance imaging
OxyHB	Oxyhemoglobin

PCA	Principle component analysis
PET	Positron Emission Tomography
SPSS	Statistical package for the social sciences
ROI	Region of interest
T	Tesla
T_1	Longitudinal relaxation parameter
T_2	Transverse relaxation parameter
T_2^*	Transverse relaxation parameter (effective)
TE	Echo time
TR	Repetition time
US	Ultrasound
VENC	Velocity encoding

1^{st}	First
2^{nd}	Second
2D	Two dimensional
α	Flip angle
D	Data matrix in PCA analysis
ϵ	Error term in hypothesis driven analysis
κ	Parameter weights hypothesis driven analysis
l	Length of active/ inactive segment in PCA analysis
m	Number of voxels in a slice
min	Minute
ml	Milliliter
n	Number time points in a BOLD set
p_k	Loading vectors in PCA
sec	Second
t_k	Score vectors in PCA
X	Idealized response matrix
Y	Data matrix in hypothesis driven analysis

Chapter 1

The Liver

1.1 Anatomy

The liver is the largest solid organ of the human body and accounts for 2-5% of the total body weight (Geller and Petrovic 2004). In the adult, the liver weighs between 1400 and 1600g (Meeks et al. 1991). It is situated in the upper right quadrant of the abdominal cavity, below the diaphragm, and is partially protected by the ribs (Shier et al. 2006).

Macroscopically, folds and fissures divide the liver into two wedge-shaped lobes: the right and the left lobe. The right lobe, which is six times the size of the left one, is further divided into a caudate and a quadrate lobe that are located on the posterior and inferior surfaces, respectively (Sherlock and Dooley 2002).

Microscopically, the hepatic organization can be described by one of two models: the classic lobule and the liver acinus (Bacon and Bisceglie 2000). In the lobular model, which is the one most commonly used, plates of hepatocytes

are arranged in a hexagonal structure, radiating outward from a central vein (Meeks et al. 1991). A portal triad, containing a hepatic artery, a portal vein, and a bile duct is located at the corners of the hexagon (Bacon and Bisceglie 2000). Flow of blood from the periphery of the lobule to the central vein is guided through vascular channels called sinusoids. In the liver acinus model, on the other hand, the portal triad is described as being surrounded by three concentric zones of hepatocytes. Zone three is the one furthest away from the triad, and thus, it obtains the most oxygen-poor blood (Meeks et al. 1991). Although these two models outline the structural liver units differently, they do not provide conflicting explanations.

The liver has a dual blood source, receiving its supply from the hepatic portal vein and the hepatic artery. Venous blood accounts for 75% of the blood conveyed to the liver, while the remaining 25% comes from the hepatic artery (Bacon and Bisceglie 2000). The portal vein carries digestion product-rich blood from the intestine, the stomach, the pancreas, and the spleen to the liver (Meeks et al. 1991). After passing through the hepatic sinusoids, this venous blood returns to the circulatory system by emptying into the inferior vena cava (Shier et al. 2006). The oxygen-rich blood, which is about a quarter of the cardiac output, is supplied to the liver via the hepatic artery (Meeks et al. 1991).

1.2 Physiology

The design of the liver, with its one-cell thick plates of hepatocytes and its hepatic sinusoid vascular system allows for maximal interaction between the blood and the hepatic cells (Meeks et al. 1991). By exposing two surfaces of the hepatocytes to the sinusoidal blood, the liver is able to efficiently carry out its vital functions. The liver plays key roles in the metabolism of carbohydrates, proteins, and fats. It stores important nutrients, including iron, vitamins and glycogen. It also synthesizes plasma proteins, participates in biochemical transformations, detoxifies the blood, and activates enzymes (Geller and Petrovic 2004). As a glandular structure, the liver secretes many substances, including bile, which is stored in the gallbladder and assists in the digestion of fat (Shier et al. 2006).

1.3 Diseases

Due to the numerous functions that the liver performs, especially those of detoxification, it can become vulnerable to many diseases. These may arise from viral invasions, bacterial infections, a poor diet or the excessive intake of alcohol. The symptoms associated with a given disease depend on its grade and its stage.

One important viral liver disorder is hepatitis. Hepatitis has been serotyped into A, B, C, D and E forms. These result in the inflammation of the liver, which can be acute, chronic or both, depending on the strain of viruses involved. Chronic infection can develop from hepatitis B, C and D viruses (Bacon and Bisceglie 2000). This may then lead to fibrosis followed by the development of cirrhosis: a situation in which the liver tissue is scarred and can no longer function properly.

1.4 Evaluation of Liver Function

In order for the liver to carry out all of its functions, any diseases that may affect its normal performance must be identified and treated. Several methods are available to detect alterations of the liver and to assess its function. A set of biochemical tests, known as liver function tests (LFTs), measure the amount of specific molecules found in a sample of blood (Sherlock and Dooley 2002). Changes in the concentrations of these molecules can indicate diseases associated with hepatocyte damage. Some of the markers that are commonly assessed include enzymes; such as alanine aminotransferase (ALT), aspartate aminotransferase (AST) and alkaline phosphatase (ALP), proteins such as albumin, and biochemical breakdown products such as bilirubin (Bacon and Bisceglie 2000). Although these laboratory tests are simple to perform,

they have limitations with regards to sensitivity and specificity. Thus, they are commonly carried out together with other diagnostic imaging examinations that consider changes in the structure of the liver, such as computed tomography (CT), ultrasound (US) or magnetic resonance imaging (MRI) (Bacon and Bisceglie 2000).

Instead of assessing liver function by analyzing the blood, a biopsy can be performed. In this procedure, a needle is inserted through the skin and a sample of liver tissue is collected. While this method looks at damage to liver tissue directly and remains to be an invaluable tool in determining liver disorders, it has some problems (Geller and Petrovic 2004). In order to successfully extract a liver sample, the patient must be able to lie still for a few seconds. This may not always be possible, given the physical fragility of some of the patients. Thus, an organ adjacent to the liver might get punctured (Bacon and Bisceglie 2000). Also, since this is an invasive procedure, complications such as hemorrhage or infections do arise. These are more common in children than in adults (Sherlock and Dooley 2002). There is a low mortality rate associated with performing a biopsy, and this is mostly because of hemorrhagic complications (Bacon and Bisceglie 2000). A liver biopsy does also provide false-negative results in some cases.

Due to the difficulties that accompany a biopsy, and the uncertainty associated with interpreting the results of LFTs, researchers have been attempting to develop reliable imaging procedures, using US, CT, PET or MRI to look at liver function.

The imaging modality that is first used to assess diffuse liver disorders is B-mode ultrasound (Abbattista et al. 2008). Doppler ultrasonogrpahy is sometimes utilized to evaluate hepatic blood flow. Many hemodynamic studies have also used contrast enhanced ultrasonography, where the intravenous administration of microbubbles results in the enhancement of flow signals. By analyzing the transit times of the injected contrast agent, research groups have been able to use this as a tool to differentiate between patients with liver cirrhosis and healthy individuals (Abbattista et al. 2008). Ultrasound elastometry has also been recently employed to evaluate liver fibrosis (Friedrich-Rust et al. 2007)(Oliveri et al. 2008). Since fibrosis is associated with an increase in stiffness, by inducing compressions and measuring tissue strain, an estimate of the hardness of the liver can be obtained. Although US is a widespread modality and has a relatively low operational cost when compared to other imaging systems, it still has limitations. In some cases, when the patient size is large, the image quality tends to be poor, making it difficult to interpret the results. In addition, some groups have shown that biologic effects, such as

enlarged intercellular spaces, dilated sinusoids and ultrastructural damage do exist in the liver of rabbits that undergo an ultrasound(Caruso et al. 2005).

When it comes to evaluating hepatic metastasis, contrast-enhanced CT is the preferred imaging modality due to its high specificity (Chezmar et al. 1988). However, the injection of iodinated agents is not always possible, due to renal insufficiency or patient's allergies. This, along with the fact that the patient must be exposed to a small dose of ionizing radiation, may limit the application of CT in evaluating the liver.

Fluorine-18-labelled fluorodeoxyglucose (FDG)-PET imaging has also been used to detect hepatic metastases, and has been shown to have the highest sensitivity, in comparison to US, CT and MRI (Kinkel et al. 2002). However, this technique's use is limited due to its high costs and non widespread availability (Oliva and Saini 2002). In addition, PET has low spatial resolution and requires the administration of a radiopharmaceutical, thereby exposing the patient to ionizing radiation.

Dynamic contrast enhanced MRI has been used by various groups to evaluate tumor vasculature. Since knowledge of whether the tumor is being perfused by means of hepatic artery or portal vein allows for choosing the appropriate treatment method, studies that characterize the hemodynamics of hepatocellular carcinoma and liver metastases have been under-

taken. By injecting a Gadolinium chelate, such as gadoterate dimeglumine, researchers have been able to quantitatively evaluate perfusion to the liver and to characterize various hepatic cancers (Abdullah et al. 2008). Gadobenate dimeglumine-enhanced MRI has also been shown to be able to detect hepatocellular carcinoma nodules that are 1 cm in diameter or larger (Choi et al. 2008).

All of the above mentioned imaging techniques are advantageous compared to blood assessment, yet suffer from some limitations when it comes to evaluating liver function. Thus, if a noninvasive, reproducible imaging technique that is safe and does not expose the patient to ionizing radiation can be developed, it might be able to complement the routine liver tests. Recent attempts, using MRI protocols such as Blood Oxygen Level Dependent (BOLD) imaging have been developed. These procedures are non-invasive and utilize endogenous deoxyhemoglobin as a contrast agent, thereby eliminating the complications associated with intravenous injections. However, like any emerging method, there are many areas that need to be further investigated to assess the reliability of these techniques in evaluating liver function.

Chapter 2

BOLD MRI

2.1 Theory

The BOLD effect has been utilized in functional MRI studies since it was first observed by Ogawa and his colleagues in the early 1990s (Ogawa et al. 1990). Although many BOLD experiments are directed at assessing the function of the brain, the technique has been recently applied to examining other organs, such as the muscle (Noseworthy et al. 2003), the kidneys and the liver (Semple et al. 2001)(Foley et al. 2003)(Shuter et al. 1995).

BOLD contrast is based on changes in the magnetic field that result from changes in the oxygenation level of the hemoglobin molecule. The magnetic properties of this molecule depend on its oxygenation state. When hemoglobin is attached to oxygen, giving rise to oxyhemoglobin (OxyHB), it becomes diamagnetic and has a weak effect on the local magnetic field (Huettel et al. 2004). Deoxyhemoglobin (DeoxyHB), which is not bound to oxygen, is paramagnetic and has a significant effect on the local magnetic field (Huettel

et al. 2004). Thus, using a pulse sequence that is sensitive to microscopic field gradients, an increase in signal loss will accompany an area of highly deoxygenated blood (Semple et al. 2001). Sequences such as the gradient-echo, which are based on T2*-weighting, are therefore commonly used in BOLD imaging (Talos et al. 2006).

The physiological basis of the BOLD effect that is observed when imaging the brain is attributed to the increase in oxyhemoglobin supply that accompanies neuronal activity (Huettel et al. 2004). When an area of the brain is activated, blood flow to that area increases. However, since the amount of oxygen delivered is more than that actually extracted, there is a relative decrease in the amount of deoxyhemoglobin, in comparison with an inactive state (Huettel et al. 2004). This results in less signal loss in the activated state.

This BOLD technique can also be extended to study the liver. Under basal conditions, there is a characteristic ratio of OxyHB to DeoxyHB in the sinusoidal bed. When physiological processes that affect the proportion of blood oxygen occur, such as changes in blood flow, blood volume or metabolism, an associated change in the amount of deoxyhemoglobin present in the vessel is evident. Since the BOLD MR signal is proportional to the ratio of oxyhem-

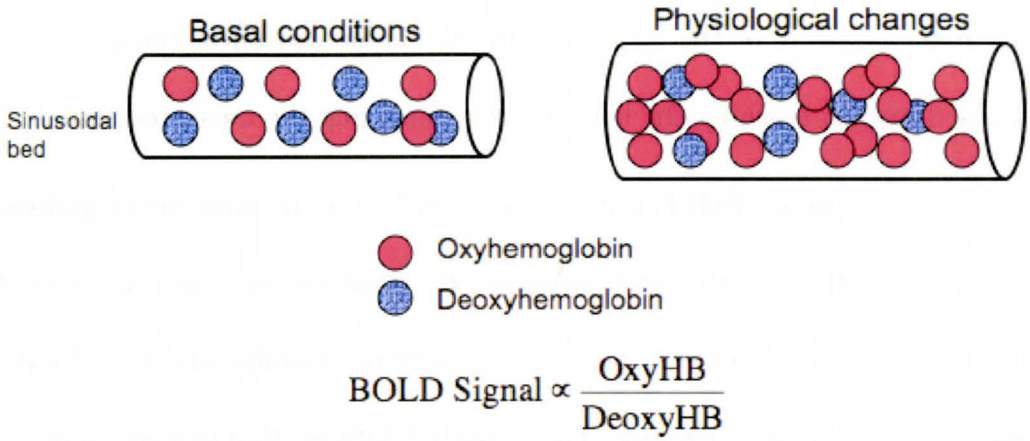

Figure 2.1: Under basal conditions, there is a certain ratio of oxyHB to deoxyHB in a blood vessel. Physiological changes alter this ratio, thereby affecting the BOLD signal.

globin to deoxyhemoglobin, oxygenation changes that accompany physiological factors have an observed effect on the measured signal (Figure 2.1)

In order to utilize the BOLD effect to look at the function of organs, an experiment can be set-up using various arrangements, one of which is a blocked design. To use this approach in the brain, for example, if one is interested in studying the visual cortex, two 30 second blocks can be employed. In the first block, which serves as the control/baseline, the subject may be asked to just focus on a spot on a blank screen. During the following 30 seconds, the subject may be asked to look at a flashing checkerboard, and this would serve as the stimulus that would cause physiological changes and alter the BOLD signal.

If trying to study the liver, the stimulus used to modulate the signal may be hyperoxia exposure or the intake of a meal. These can affect the proportion of blood oxygen reaching the liver, thereby changing the measured signal.

The collected BOLD data, which can be one or more slices gathered over time as the experimenter presents the stimulus, are then analyzed to find if there is a relationship between the applied stimulus and the observed changes in the organ of interest. This collected data set that consists of images in temporal order is referred to as the time-series. There are two ways in which the BOLD time-series can be analyzed: hypothesis driven analysis, which is the most common approach (Huettel et al. 2004), and data driven analysis.

2.2 Hypothesis Driven Analysis of the BOLD Time-series

In order to analyze the BOLD data using the hypothesis driven technique, an idealized waveform, which represents the hemodynamic response of the region being studied, must be assumed. Since the researcher is applying a stimulus and expecting to observe changes during this application, an estimate of the BOLD signal that each voxel should exhibit in response to the task must be generated. For instance, if an experiment has 2 repeating blocks, each having 30 seconds duration, and the task is performed during the

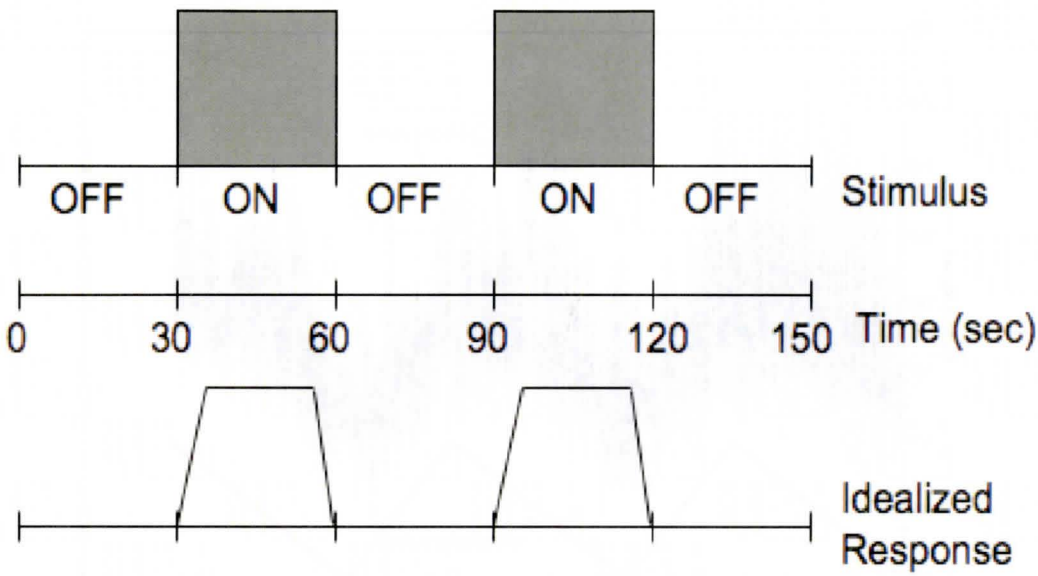

Figure 2.2: A sample block design and the idealized waveform.

second block, then the researcher might hypothesize that during the second block, an increase in the BOLD signal will be observed relative to that seen in the first block and this would allow for the development of an ideal response (Figure 2.2)

Once a model is estimated and the BOLD time-series is collected, the goal of the hypothesis driven analysis is to find voxels in the region under investigation that exhibit changes in the BOLD signal that match the changes predicted by the model. Figure 2.3 shows the collected BOLD signal from two sample voxels, one that matches the prediction of the model and one that does not, along with the idealized response.

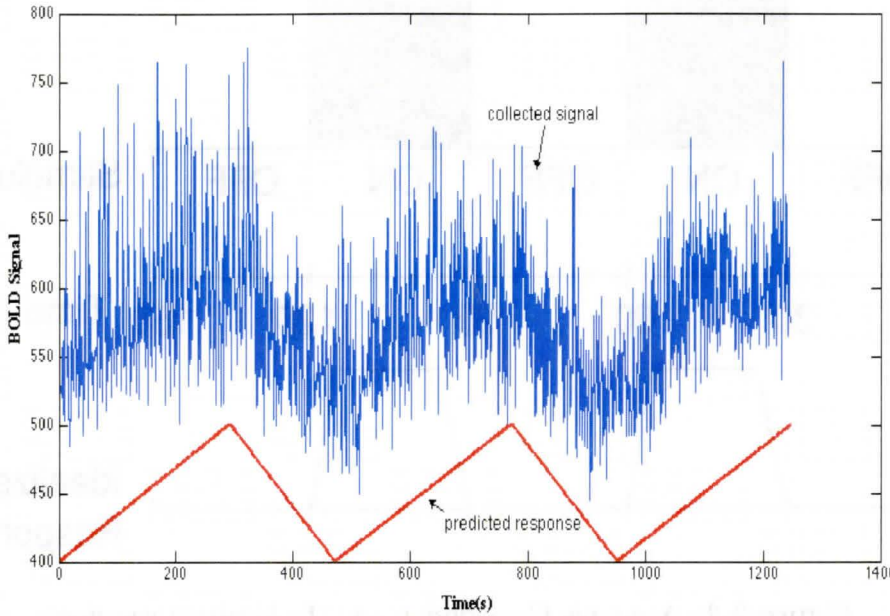

(a) A voxel whose time-series matches that predicted by the model.

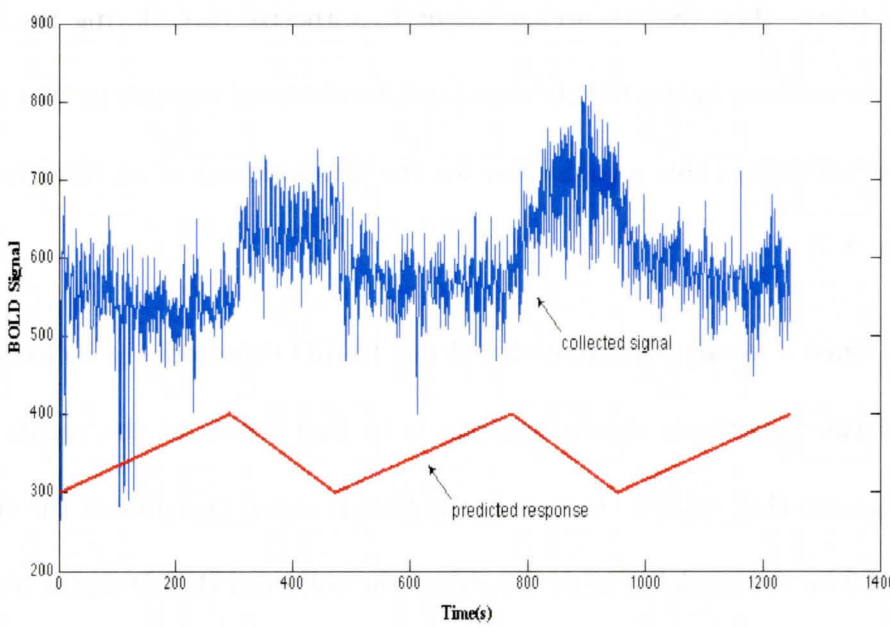

(b) A voxel whose time-series does not match that predicted by the model.

Figure 2.3: Collected BOLD time-series and the predicted response for a case where the time-varying signal fits the model (2.3(a)) and one where it is not a good fit (2.3(b))

Mathematically, the collected data from all of the voxels in the chosen slice (the time-series of all of the voxels in the imaged slice) can be arranged into a data matrix, Y. This observed data can then be represented using a general linear model as shown in Equation (2.1), where X is a matrix of the idealized response, ϵ is a matrix of the noise or an error term and κ is a matrix of the parameter weights. These weights measure the contribution of the predicted model to the observed data (Huettel et al. 2004). The goal of the general linear model is to calculate the parameters (determine the κ values) that best explain the observed data (Y) in terms of the predicted model (X) while minimizing the error term (ϵ).

$$Y = \kappa X + \epsilon \tag{2.1}$$

Once the parameter weights are calculated using the regression model in Equation (2.1), a t-statistic is obtained by dividing κ for a given voxel by its residual error (Huettel et al. 2004). The p-value corresponding to this t-statistic is then determined. If the p-value is lower than the preselected threshold, then the voxel is considered to show statistical significance and is thus said to well fit the hypothesized hemodynamic response.

Although this hypothesis driven analysis is most commonly used by researchers performing fMRI experiments, the approach has some limitations.

First of all, if a complex experiment is to be developed, it might be impossible to create an ideal waveform that best explains the expected changes that will accompany the stimulus. In addition, even if one could come up with a predicted response, it might not be an accurate one (Huettel et al. 2004). Thus, since this technique relies on modeling the collected signal in terms of the ideal hemodynamic response, if the predicted response is not accurate, wrong conclusions might be made. A model free approach has been used by some researchers to overcome these difficulties.

2.3 Data Driven Analysis of the BOLD Time-series

The data driven analysis is a technique that tries to find patterns in the BOLD time-series that might be related to the application of the stimulus. This is sometimes known as an exploratory analysis (Huettel et al. 2004) as the researcher investigates the underlying data structure and attempts to extract important task-related features. In order to find the underlying components that characterize the fMRI data, a few techniques have been used, including principle component analysis (PCA) (Anderson et al. 1999). In PCA, a set of variables, which are orthogonal to each other and are known as principal components, are initially generated. The collected fMRI data is transformed

into a new feature space that is created from these principle components. The resulting transformed data set contains time-series that are sorted based on directions in the data that have maximal variance (Suma and Murali 2007).

The mathematical formalism of this technique can be explained as follows. Let the collected BOLD data be made up of a single slice that has n time points and m voxels. A data matrix, D can then be constructed with dimensions $n \times m$, where the rows represent the data in time (the time-series) and the columns represent the data in space (the voxels) (Anderson et al. 1999). Calculating the sample covariance matrix, $D^T D$, results in a square matrix having the dimensions of $m \times m$. The eigenvectors of this covariance matrix, which are known as the loadings, and the eigenvalues can then be computed. By organizing the m loadings in decreasing order of their corresponding eigenvalues, the principle components of the data set can be found. The first principle component explains the direction in the data that has the largest variance, and the successive components represent the remaining directions arranged in order of their significance (Suma and Murali 2007). The final step requires constructing a feature space from the most dominant principle components and representing the original time-series in terms of this new variable space, resulting in vectors known as scores.

The decomposition of the data matrix into loadings and scores can be written using the PCA equation (Equation (2.2)), where D is the data matrix, t_k are the score vectors and p_k are the loadings (Geladi and Grahn 1996).

$$D = \sum_{k=1}^{K} t_k p_k^T \tag{2.2}$$

Although the data driven analysis technique does not rely on estimating the hemodynamic response of the region being studied, there are certain challenges that accompany its use. For instance, it is not always straightforward to decide how many principle components should be used to model the data. Using less components allows for reducing the dimensionality of the data, but it may result in missing some of the variance in the original data (Huettel et al. 2004).

2.4 Applying the BOLD Effect to the Evaluation of Liver Function

The BOLD contrast has been used by a number of researchers to assess liver function. Although many BOLD experiments have been undertaken to evaluate the function of the brain, the extension from neuronal studies to those dealing with the liver reveals that the BOLD contrast is further enhanced in the liver due to its vasculature. Since the liver contains a higher blood volume

than the brain, it is more sensitive to changes in oxygenation, and thus, changes in liver signal intensities are higher than those observed in brain studies (Foley et al. 2003).

2.5 Literature Review

A few groups have utilized the BOLD contrast to assess changes in liver tissue oxygenation that accompany various challenges. Foley et al investigated the effect of alcohol consumption on hepatic microvasculature using male Wistar rats (Foley et al. 2003). After dividing the rats into a control group and a chronically-ethanol treated one, a spin echo pulse sequence was used to acquire images following the exposure of the rats to normoxic, hyperoxic, hypoxic or hypercapnic conditions (Foley et al. 2003). The study found that challenges that resulted in an increase in the oxygenated blood entering the vessels were accompanied by an increase in signal intensity on the T2-weighted images, as expected (Foley et al. 2003). The results also indicated that there was a microvascular dysfunction in the treated rats, since their images showed less signal changes following the challenges, when compared to the control rats (Foley et al. 2003).

Semple et al studied fetal oxygenation before and after the mother breathed O_2 for twenty-minutes (Semple et al. 2001). Analysis of a region

of interest selected from the liver of the fetus indicated that there was a significant increase in the measured T2* value in the BOLD images that were acquired following the O_2 breathing in seven of the nine healthy subjects tested (Semple et al. 2001). The study concluded that this technique may be useful in detecting placental dysfunction resulting in insufficient delivery of oxygen to the fetus (Semple et al. 2001).

Shuter et al investigated the effects of sacrifice on the MR signal by measuring the T1, T2 and T2* of the liver, kidney and brain before and after sacrifice of Wistar rats (Shuter et al. 1995). A reduction of the T2* values was observed in all three organs postsacrifice, indicating that as the deoxyhemoglobin content increased in the blood, a change in the susceptibility resulted, which was manifested as a decrease in the MR signal.

Noseworthy et al tested the effect of cycling between 100% O_2 and 20.8% O_2 on the oxygenation of the human liver (Fan 2006). They also investigated whether a fasted liver can show BOLD signal changes following the intake of a can of Ensure Plus®. In addition, they collected the BOLD signal during the ingestion of the meal and tried to determine if any useful information regarding liver meal response can be obtained from that data. The reason behind deciding to analyze the BOLD signal following meal intake is that earlier work done by Noseworthy et al demonstrated alterations in the

oxygenation of the liver parenchyma when comparing fasted and postprandial states (Noseworthy et al. 1999). A decline in the BOLD signal after the intake of a meal has also been shown on T2*-weighted images (Fan et al. 2006), suggesting that BOLD signal changes may provide information about liver function.

The hyperoxia cycling data collected from their experiments showed positive enhancement in most of the healthy individuals that participated in the study, while some subjects showed negative enhancement and some did not show any enhancement (Fan 2006). In addition, by comparing the postprandial data to that obtained before the intake of the meal, their results showed that for subjects with positive enhancement, significant reduction in the enhancement was evident after the intake of the meal. However, for the subjects that did not show positive enhancement, there were no observed significant changes between the two states (Fan 2006). Although their challenge did not provide consistent results among all the healthy subjects, the novel BOLD approach that they developed raised the possibility that functional assessment of the liver may be achieved using BOLD MR Imaging.

Chapter 3

Problem Definition and Hypothesis

3.1 Problem Definition

The liver plays important roles in biochemical transformations and blood detoxification. Although various techniques are now available to evaluate liver function and detect diseases that may alter its performance, they all have some drawbacks: they are either invasive, have limitations with regards to sensitivity and specificity, involve the injection of a contrast agent, or expose the patient to ionizing radiation. Thus, if a noninvasive, reproducible and safe imaging technique can be developed, it might be able to complement routine liver tests. A few groups have demonstrated that Blood Oxygen Level Dependent (BOLD) imaging may be used to study liver tissue oxygenation. This technique is non-invasive and relies on endogenous deoxyhemoglobin as a contrast agent, thereby eliminating the complications associated with intravenous injections. Although these studies show promising results, a reliable procedure has yet to be developed to evaluate liver function.

3.2 Hypothesis Statement and Proposed Solution

The objective of this project is to use BOLD MRI in the functional assessment of the human liver. A former member of our group has previously developed a liver challenge procedure that relies on modulating the BOLD signal with hyperoxia and meal intake (Fan 2006). Although the original protocol was tested on healthy subjects, inconsistent results were obtained. In addition, due to time limitations, patient recruitment was not possible. Thus, further work is needed in order to make statistically significant conclusions about the possibility of detecting liver disease using the BOLD procedure.

A brief description of the method that was employed is given here. A more thorough explanation can be found elsewhere (Fan 2006). The technique involved imposing two challenges that alter the oxygenation of hepatic blood; exposure to 100% O_2 and ingestion of a can of Ensure Plus®. BOLD images were collected during the hyperoxia cycling sessions, which occur pre and post intake of the meal. Image data was also gathered during food ingestion.

Since the available challenge did not provide consistent results among all healthy subjects, the first purpose of this project was to make any changes that could optimize the current technique. This included changes in the experimental set-up as well as data analysis. In the original protocol, hypothesis

driven analysis was employed to analyze the collected BOLD data. Since the liver has a dual blood supply, it is hypothesized that using a model-free approach may be more accurate when it comes to evaluating changes that accompany the applied stimuli in this organ due to its complex blood supply. In addition, it is postulated that since physiological changes alter the BOLD signal, in order to optimize post Ensure BOLD acquisition, the data should be collected when there is maximal blood flow, as opposed to immediately after intake. Furthermore, since calculating the percentage of the liver that was responsive in the pre and postprandial states and performing a t-test to compare them did not prove to be a good detection measure, it may be more appropriate to calculate the percentage difference between the responsive pixels in the pre and postprandial states.

The second purpose of this project was to test if the technique can differentiate between healthy livers and those of individuals with liver disorder, especially those with Hepatitis C. Based on studies that have looked at the effects of meal intake on the BOLD signal in healthy livers (Noseworthy et al. 1999)(Fan et al. 2006), it is hypothesized that, healthy livers will show a decrease in their hyperoxia-induced BOLD contrast post-prandial, in comparison to the pre-intake response. Diseased livers, on the other hand, are postulated

to respond differently; either showing an increase in response to the meal, or no significant change due to food ingestion.

Chapter 4

Materials and Methods

4.1 MR Scanner

All MR imaging was performed using the GE Signa HD 3-Tesla short-bore MR imaging system (General Electric Healthcare, Milwaukee, WI) located at the Imaging Research Center of the Brain-Body Institute, St. Joseph's Healthcare, Hamilton, Ontario, Canada. Experiments were performed in the early morning following an overnight fast. An eight-channel torso phased array coil (USA Instruments In., Aurora, OH, USA) was used to receive the signal while the body coil was used for transmitting the radio frequency pulses. All experiments in this study were approved by the St. Joseph's research ethics board (REB) in accordance with the declaration of Helsinki.

4.2 Blood Flow

This was a preliminary study undertaken to investigate the effects of meal ingestion on hepatic portal vein flow.

4.2.1 Accessories

Peripheral pulse gating was employed in this study to monitor the cardiac cycle and provide a way of triggering while the data was being acquired.

4.2.2 Protocol

All subjects were examined in the supine position and they were placed feet first into the magnet bore. Flow measurements were performed during breath holding using a vascular fast 2D phase contrast pulse sequence that was commercially available. Images were collected for sixteen consecutive cardiac phases using a velocity encoding strength (venc) of 40cm/s for the hepatic portal vein (α =20°, TR automatically set based on heart rate of subject). The imaging plane was prescribed perpendicular to the vessel of interest. Three baseline MR flow measurements of the portal vein were acquired after an overnight fast. Following acquisition of the fasting images, subjects consumed a standardized meal (one can of 235ml of Ensure Plus®,Abbott Laboratories, Saint-Laurent, Qc) while remaining in their original supine position in the scanner. Images of the hepatic portal vein were collected immediately following food intake and in ten-minute intervals up to fifty minutes postprandial.

4.2.3 Subjects

Four healthy human subjects (mean age: 33±6 years) participated in this preliminary study. None of the participants had a history of liver or cardiac disease or were on long-term medication use. Informed consent was obtained from each subject prior to the examination.

4.2.4 Data Analysis

Blood flow in the vessels was measured using the CV Flow software package that was commercially available on the GE Advantage Windows (AW) workstation (AW 4.2_03). A separate region of interest (ROI) was manually drawn around the chosen vessel on the magnitude image for each of the frames in the cardiac cycle. This ROI was then applied to the phase images and a flow rate was calculated for each of the cardiac phases by multiplying the contoured area of the vessel with the mean flow velocity in the vessel. The volumetric flow rate over the cardiac cycle was then determined by averaging the flow rates from all of the frames. The collected data was entered into a spreadsheet and statistical analysis was performed using computer software (SPSS for analysis, Excel for plots). The Paired Student t-test was used to compare the basal flow to that following meal intake.

4.3 BOLD Experiments

These BOLD examinations were performed to test the response of the liver to two challenges: hyperoxia cycling and the intake of a meal.

4.3.1 Accessories

A respiratory bellows, which is a pneumatic elastic belt, was used to monitor the subject's breathing activity. For most subjects, this was placed around the chest. However, for subjects that were heavy stomach breathers, the bellows was put closer towards the stomach area.

For the hyperoxia cycling part of the experiment, 100% O_2 and medical air (20.8%O_2) were supplied to the subject through a face mask. The mask was connected to the hospital oxygen supply. Our cycling was employed by manually switching between O_2/ medical air within the scan room.

For the meal ingestion part of the study, one can of 235ml of chocolate-flavoured Ensure Plus® (Abbott Laboratories, Saint-Laurent, Qc) was given to subjects as they laid in the supine position on the MR table. The contents of the can were poured into a plastic cup, and a person was required to enter the room and place a straw in the subject's mouth to allow for the fluid to be sipped out of the cup.

4.3.2 Protocol

In order to choose the appropriate region of the body for the BOLD study, a 3-plane localizer was initially used (a standard beginning for all MRI exams). A fast spin-echo (FSE) pulse sequence is typically employed for localization. Since this sequence is optimized by the vendor, the scan parameters were automatically set.

An axial Fast Imaging Employing Steady-state Acquisition (FIESTA) scan was then applied through the liver for the purpose of localizing subsequent scans with more clarity. This required breath-holding from the subject, which usually lasted for about 20 seconds. The subject received clear breathing instructions from the technologist.

From the acquired axial FIESTA images, the slice that showed the first bifurcation of the right hepatic portal vein was selected. Six 8mm thick sagittal FIESTA slices were then prescribed to the right of the bifurcation (TE= 1.2ms, TR automatically set, α =30°, 8mm slice thickness, 256 × 256 matrix size). This was followed with acquisition of six sagittal GRE-EPI images (TE= 35ms, TR= 1000ms, α =90°, 8mm slice thickness, 64 × 64 matrix size) at the same slice locations. One slice was finally chosen from these slices and was used in subsequent BOLD experiments. The slice had to satisfy a few criteria in order to be chosen: it had to contain a big volume of liver with a reasonable signal

intensity and show the kidney border. The BOLD time series imaging was then performed using a single-shot GRE-EPI sequence on the selected slice and the time-series data was collected (with the same parameters as above).

4.3.3 Liver Challenge Procedure

Hyperoxia cycling and meal intake were used as challenges to study liver response. Two protocols were tested, both of which involved switching inspired gases between hyperoxia (100% O_2) and normoxia (medical air: 20.8% O_2), with each having 3 hyperoxia phases. In the first experiment, hyperoxia was cycled 3 times, each time being 3 minutes long. These were separated by 5 minutes of normoxia (Figure 4.1). The second experimental protocol was reversed; that is hyperoxia was cycled 3 times but for periods of 5 minutes in duration, and these were separated by 3 minutes of normoxia (Figure 4.2). Both experimental protocols lasted twenty-one minutes and eight seconds and resulted in the acquisition of 1248 images. The first twenty seconds consisted of discarded images.

Following image acquisition, the subject's liver was challenged by meal intake. No images were collected during ingestion. Previous work showed that images that were acquired during the meal consumption were too varied and resulted in high degree of inconsistency between and even within the same

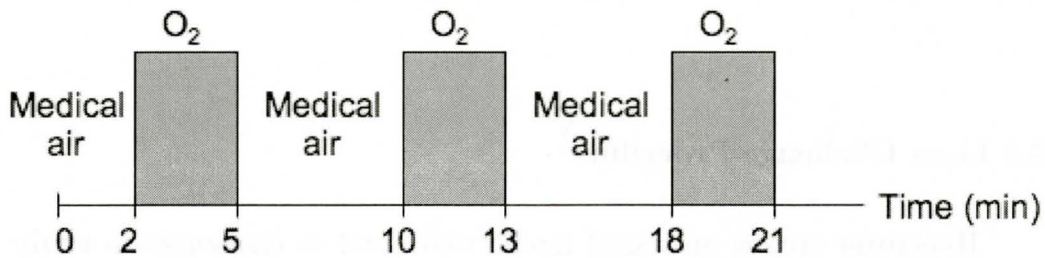

Figure 4.1: Model 1 a timing diagram of the gases that were cycled through to induce changes in liver oxygenation.

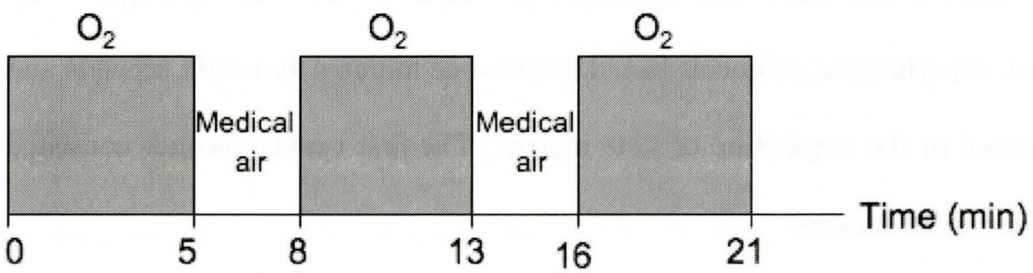

Figure 4.2: Model 2: a timing diagram of the gases that were cycled through to induce changes in liver oxygenation.

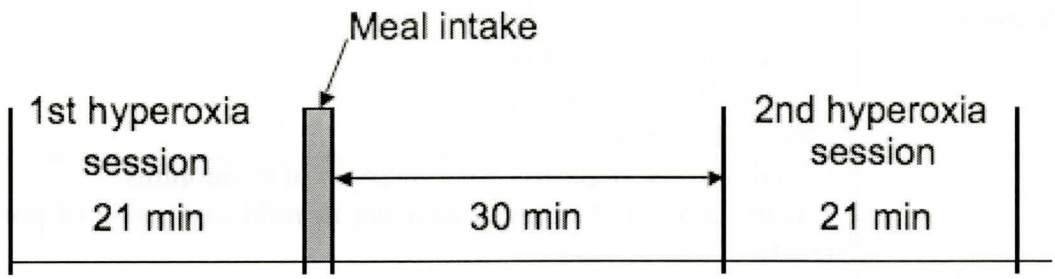

Figure 4.3: Timing diagram for the entire BOLD imaging procedure including both hyperoxia sessions and meal intake.

subject (Fan et al. 2007) Therefore, postprandial imaging was done when blood flow in the HPV was maximal (i.e. thirty minutes post ingestion) At this time, the gas cycling experiment was repeated. It should be noted that if the first model (Figure 4.1) was used for a given subject in the pre-intake session, then this same model was employed postprandial. Similarily, using the second model (Figure 4.2) in the initial session required that this same model be used following food intake. Figure 4.3 shows the timing of the BOLD imaging sessions after the localization data was collected.

4.3.4 Subjects

Eight healthy human subjects (mean age: 30±7 years) were studied using model 1 hyperoxia set-up (Figure 4.1) and three healthy human subjects (mean age: 27±5 years) participated in the study using model 2 (Figure 4.2)

Patient Number	Diagnosis
1	- Mild chronic hepatitis - Grade 2 inflammation - Stage 1 fibrosis
2	- Mild chronic hepatitis with increase of eosinophils - Mild increase of fibrosis resulting in mild expansion of portal tracts - Chronic inflammatory infiltrate
3	-Chronic hepatitis - Stage 3 fibrosis - Possible cirrhosis
4	-Mixed macro and micro cirrhosis
5	- Hepatocellular carcinoma
6	- Cirrhosis and steatosis

Table 4.1: Diagnoses of the patients that took part in the study.

One of the healthy participants in this group was examined twice: once with the second hyperoxia cycling session commencing immediately at the end of the meal intake and on another day where the hyperoxia session began thirty-minutes post intake (Figure 4.3). In addition, six patients with biopsy-proven liver disease took part in the liver challenge. Three were studied using the first model (mean age: 54±8 years) and three were studied using the second model (mean age: 63±7 years). The diagnoses of the recruited patients are shown in table 4.1. Informed consent was obtained from all subjects prior to the examination and all subjects participated in the entire study (Figure 4.3). None of the healthy participants had a history of liver disease.

4.3.5 Data Analysis

4.3.5.1 Motion Track

Although subject movement was minimized during the scanning sessions, the liver constantly moves with respiration. Thus, the collected BOLD time-series were initially corrected so that all the images from one session were spatially aligned in time (i.e. voxel one in BOLD image one described the same anatomical region as voxel one in all the remaining BOLD images). In order to track liver motion, an in-house software developed in C (Realtime MRI Motion Tracker) was used. The algorithm is based on a correlation coefficient motion tracking technique. This was originally developed by Sussman and Wright (2003) to track coronary artery motion. However, Noseworthy et al. (2007) showed that the technique could also be applied to track the motion of the liver. Briefly, the matching algorithm is based on finding the location of a template in each of the images in a time-series by determining the position where the correlation coefficient is maximized. In order to use this technique in the liver, a template of size 32×32 is manually chosen from a reference image in the series. The algorithm then tries to find the best location of this template in all the subsequent images by calculating the correlation coefficient between this template and regions of equal size in the remaining images. The

location with the maximum correlation coefficient is chosen as the most probable position of the template. Figure 4.4 shows a snapshot of the program while it was tracking the motion of a template within the liver.

Once the position of the template was found, the corresponding 32 × 32 region was extracted from the BOLD time-series, resulting in a data set that was registered across time. This step was carried out using Matlab (Ver. 7.4.0, The MathWorks, Inc., USA). The registered BOLD data set was then analyzed using both hypothesis driven analysis and data driven analysis to investigate the effects of hyperoxia and the intake of a meal.

4.3.5.2 Hypothesis Driven Analysis of the BOLD Time-series

Using the hypothesis driven technique, an idealized waveform had to be initially created. Figures 4.5 and 4.6 show the model response function that was predicted to match the stimulus for set-up 1 and set-up 2, respectively.

To analyze the collected data using this approach and determine the response of the liver, the registered BOLD time-series obtained following the motion correction step and the predicted waveform were inputed into the FEAT (FMRI Expert Analysis Tool) algorithm (Version 4.0), which is part of the FSL (FMRIB's Software Library, http://www.fmrib.ox.ac.uk/fsl/) package.

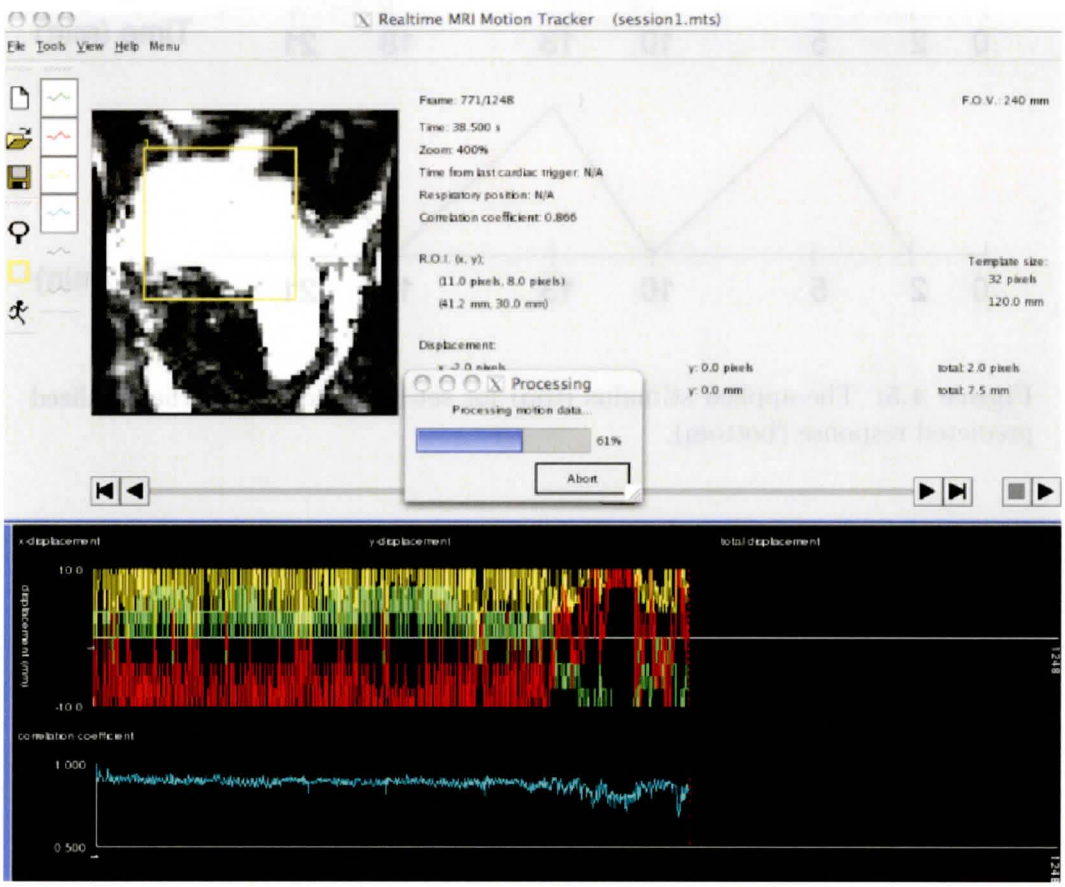

Figure 4.4: The motion tracking program. by choosing a liver region to be tracked (area enclosed by the yellow box in the image), the algorithm calculated the position of the template that maximized the correlation coefficient.

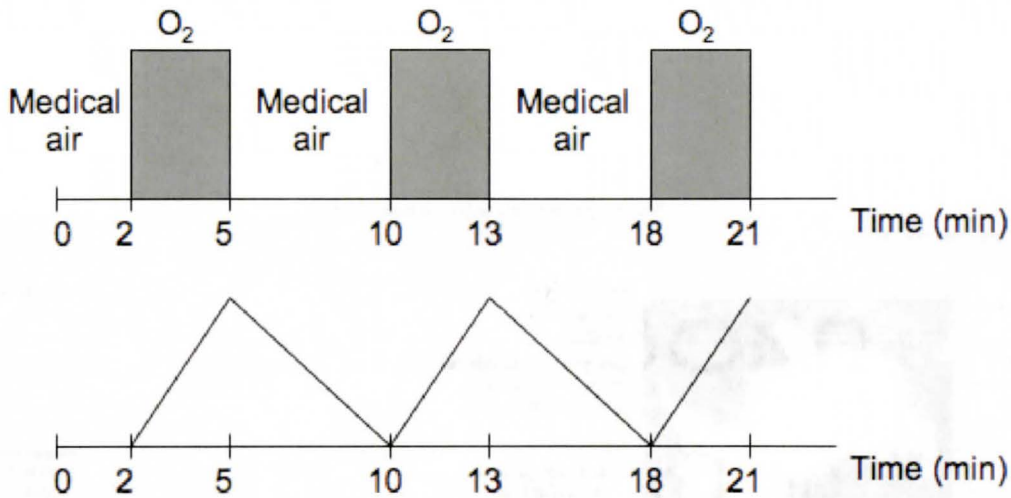

Figure 4.5: The applied stimulus (top) for set-up 1 along with the idealized predicted response (bottom)

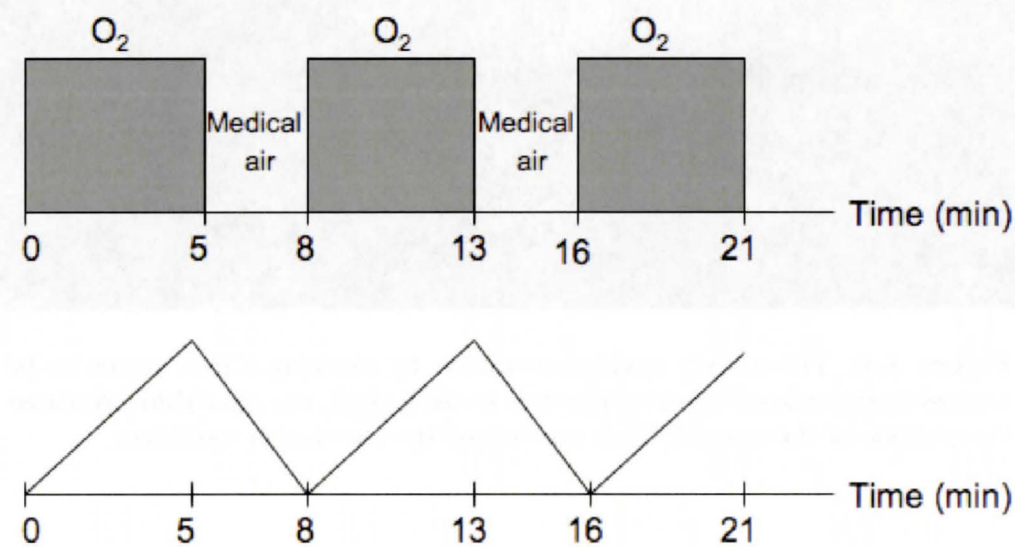

Figure 4.6: The applied stimulus (top) for set-up 2 along with the idealized predicted response (bottom)

This is a model-based analysis tool that employs a general linear model (GLM) to find voxels that exhibit changes that are matched to the changes predicted by the hypothesized model. The program generated z statistic images, where pixels that had z scores corresponding to p-values less than 0.05 (thresholding was set to 0.05 in these experiments) were considered to show statistically significant correlation with the ideal model.

4.3.5.3 Data Driven Analysis of the BOLD Time-series

Local principal component analysis (PCA) was employed to extract patterns from the BOLD data series that were related to the application of the stimulus. The technique used was an extension of work done by Lai and Fang (1999). In order to perform local PCA, the time-series data was initially divided into two segments, an active one (during the application of 100% O_2) and an inactive one (during the application of medical air). These segments were taken from the center of each of the regions to avoid data from the transition periods that may be associated with errors. The selected segments all had equal length. Figure 4.7 shows these regions in grey for both model 1 and 2 set-ups. Note that it was not necessary to know the shape of any hypothesized waveform in this type of analysis. All that was required was that two different states exist, where the two states were dissimilar. Thus,

for each voxel, three hyperoxia segments and two normoxia segments were chosen. In the first model, the length of each of these segments was 120 time points, and in the second model, it was 140 time points. If local principle component analysis was performed using a single voxel, then the dimensions of the data matrix would have been $5 \times l$ (where 5 corresponds to the sum of the 3 active and 2 inactive segments and l represents the length of these segments (i.e. 120 or 140, depending on the set-up used)). However, local principle component analysis was performed on segments that were in the neighborhood of each voxel (i.e. the center voxel with its eight neighboring voxels). The data matrix for each voxel thus had the dimensions of 45×120 and 45×140 for model 1 and model 2, respectively. The first 27 rows of the data matrix contained the active time-series while the last 18 rows contained the inactive time-series. After carrying out the decomposition using principle component analysis, the two dominant components for each of the voxels were selected and the feature space was formed. By projecting the data from the 45 time-series onto this new subspace, it was assumed that two separate clusters can be formed, one for the data in the active segments and one for the data in the inactive segments. The Bhattacharyya distance was finally used to determine the degree of separability between the centers of these two clusters (Theodoridis and Koutroumbas 2003). By carrying out the above mentioned

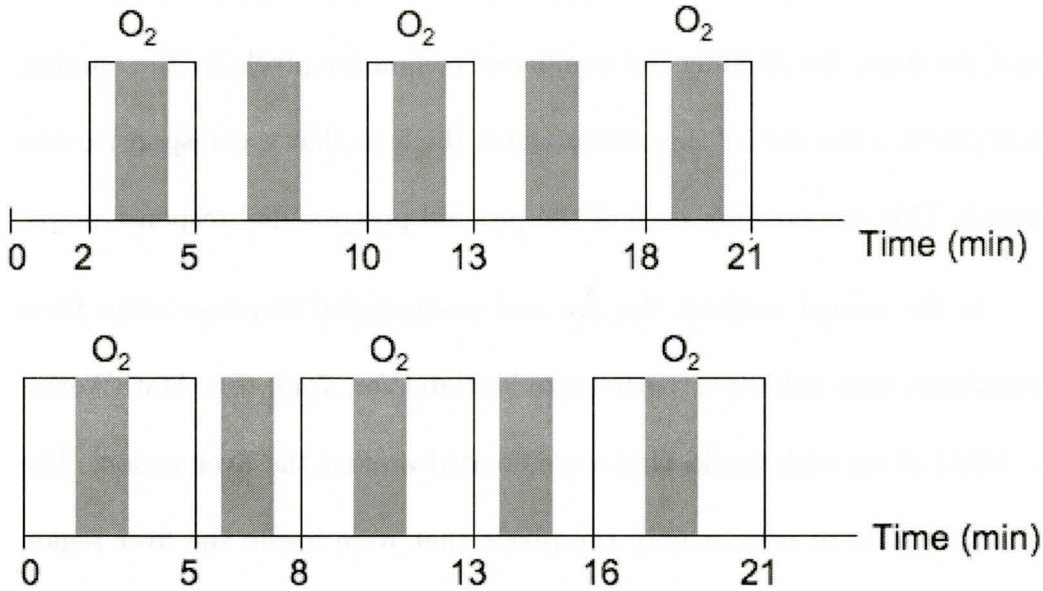

Figure 4.7: The selected segments (shown in grey) for the data driven analysis for the first model (top) and the the second model (bottom)

analysis for each of the voxels in the image, a response map was obtained similar to that in the hypothesis driven analysis. Data driven analysis was computed using Matlab (Ver 7.4.0, The MathWorks, Inc., USA)

4 3.5.4 Determining Liver Response

In order to determine the response of the liver to the applied stimuli, two approaches were used. In the first method, the response map that was generated from the analysis of the BOLD time-series was imported into Matlab (Ver 7.4.0, The MathWorks, Inc., USA) and the responsive pixels were

counted. The total number of liver pixels was also determined by contouring around the liver. By dividing the number of responsive pixels by the number of liver pixels, a measure of the percentage of the liver that was responsive was obtained. This was done for each of the pre and postprandial response maps.

In the second method, the pre and postprandial response maps for a given subject were initially imported into Matlab (Ver. 7.4.0, The MathWorks, Inc., USA) along with masks that were created around the liver region. The masks were used to extract only the pixels that were inside the liver region from the response maps. A t-test was then performed between the means of the pre and post intake response maps for a given subject to determine if there was a statistically significant effect of the meal on the response of the subject. The difference in the means of the response values between the two states (post intake - pre ingestion) was calculated and this was turned into a percentage difference by normalizing by the pre intake values and multiplying the resulting number by 100 to get a percentage. Thus, a p-value (from the t-test) and the percentage difference in the means of the responsive pixels between the extracted responsive pixels from the pre and post intake images were computed.

Chapter 5

Results

5.1 Blood Flow

5.1.1 Baseline Hepatic Portal Vein flow

The basal flow values for each of the subjects before the ingestion of the standardized meal were initially determined. The average pre-intake flow in the portal vein was found to be 1312.8 ml/min with a standard deviation of 267ml/min.

5.1.2 Operator's Error

Intra-observer variability was determined by contouring the same exam set on three different days. In all cases, the variation was evaluated and found to be less than 5.1%.

5.1.3 Variation within Subject

Intra-individual variability was determined by comparing data obtained by repeating the experiment on the same subject on two different days. A variation of 16.6 % was found between these measurements.

5.1.4 Effect of Intake of Ensure Plus®

The ingestion of a can of Ensure Plus resulted in an increase in hepatic portal vein blood flow for all subjects. This was found to be significant at all intervals following intake ($P<0.004$) as shown in Figure 5.1. The largest increase in flow, relative to the baseline value (70.5%) was seen thirty minutes following meal ingestion (Table 5.1).

Time following intake (minutes)	Change from baseline measurement (%)
0	0
1	19.9
10	45.7
20	68.6
30	70.5
40	65.2
50	46.2

Table 5.1: Percent change in portal vein blood flow

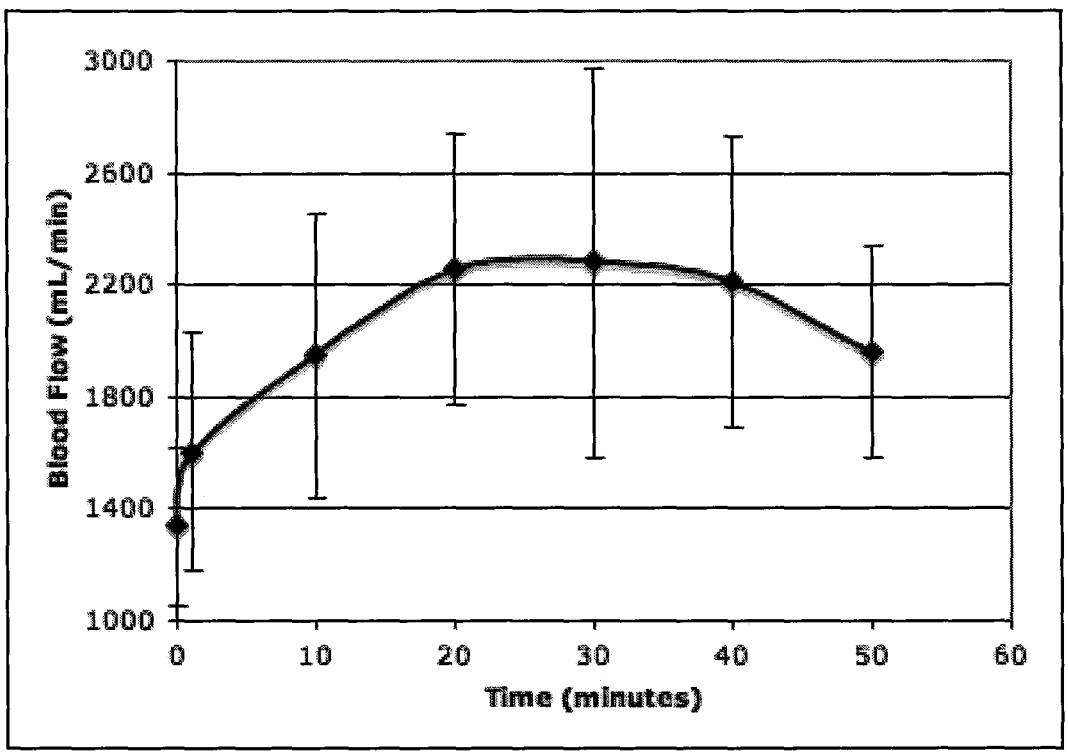

Figure 5.1: Blood flow in the portal vein before and after the intake of a can of Ensure Plus®. Results are shown as a mean and standard deviation. Significant changes from baseline measurements were noted at all intervals ($P<0.004$).

5.2 BOLD Experiments

5.2.1 Hypothesis Driven Analysis (GLM)

In this section, the results of the experiments conducted using hypothesis driven analysis will be presented.

5.2.1.1 The First Hyperoxia Model (Gas Cycling Model 1)

Using the GLM to analyze the first gas cycling approach, three healthy subjects (out of 8) were found to exhibit a decrease in BOLD signal intensity with application of 100% O_2 (i.e. their response was the exact opposite of that depicted in figure 4.5). These subjects are referred to as negative responders and the ones that showed the hypothesized expected increase in signal intensity with 100% O_2 are referred to as positive responders. Figure 5.2 shows a sample time-series from one subject whose BOLD signal exhibited the unpredicted behavior. A sample response from a subject with expected signal intensity increase is also shown in the same figure for comparison.

In the first analysis technique, the percent of liver that was modulated by inspired gas was determined for all subjects. Table 5.2 shows the results

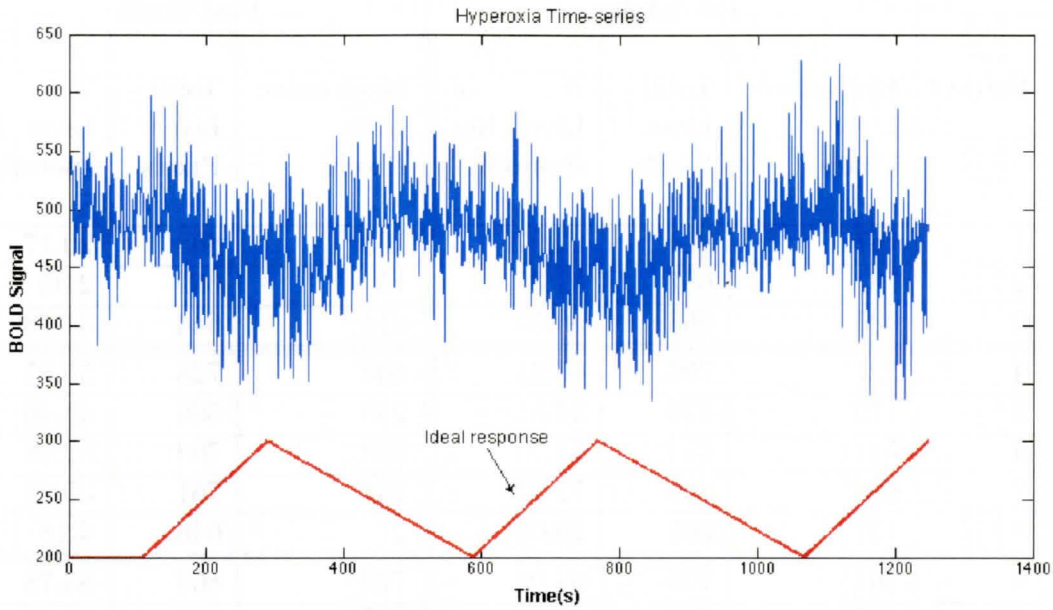

(a) A sample time-series from one subject whose BOLD signal decreased with breathing 100% O_2

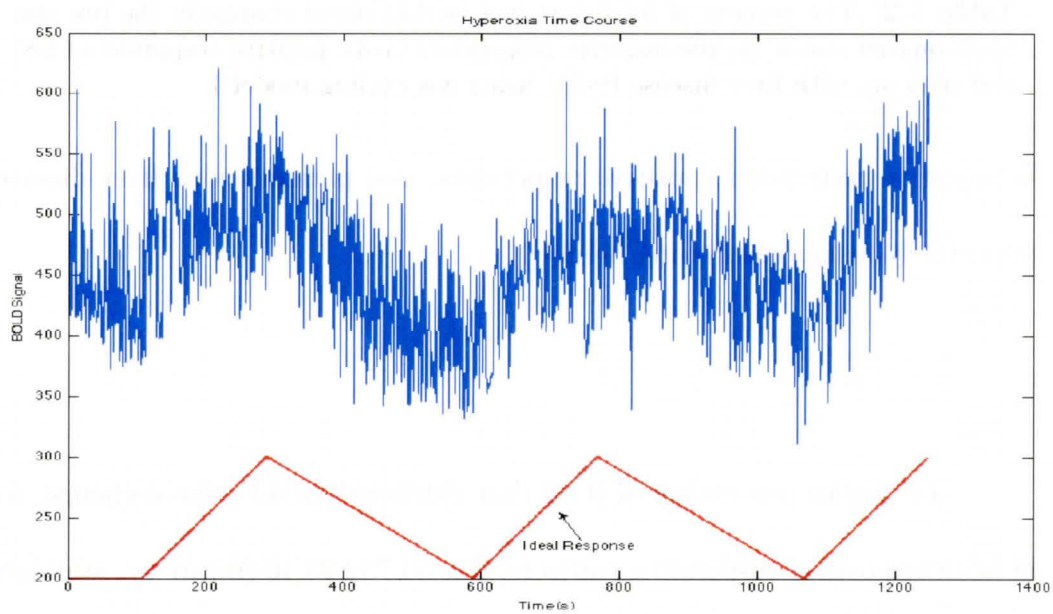

(b) A sample time-series from one subject whose BOLD signal increased in intensity with 100% O_2 administration.

Figure 5.2: Two time-series representing a negative responder (5.2(a)) and a positive responder (5.2(b)) obtained using gas cycling model 1 (i.e. 3 phases of 3 minutes 100% O_2 separated by 5 minutes of normoxia)

	Pre intake			Post intake		
Subject	Responsive Liver Pixels	Total Liver Pixels	% of Liver Responding	Responsive Liver Pixels	Total Liver Pixels	% of Liver Responding
1	187	814	22.97	163	808	20.17
2	78	687	11.35	15	639	2.35
3	335	663	50.53	211	644	31.78
4	527	796	66.21	403	728	55.35
5	179	476	37.61	246	566	43.46
6	541	754	71.75	369	703	52.48
7	628	866	72.52	268	761	35.22
8	137	665	20.60	27	646	4.18
9	461	720	64.03	723	863	83.78
10	367	769	47.72	325	519	62.62
11	703	928	75.75	671	921	72.54

Table 5.2: The percent of liver that had BOLD signal change in the pre and postprandial states for the negative responders (1-3), positive responders (4-8) and patients with liver disease (9-11) using gas cycling model 1.

for negative responders, positive responders, and patients with liver disease, respectively, using gas cycling model 1.

The mean percentage of liver that exhibited BOLD signal change, for all healthy positive-responding subjects, was 53.73±23.40 (mean +/- standard deviation) in the pre intake session and 38.14±20.57 in the postprandial session. These differences were statistically significant ($P < 0.05$, paired student t-test). The negative responders, on the other hand, showed no significant dif-

ference between the two states (mean percentage of liver responding pre intake: 28.28±20.12, mean percentage of liver responding post intake: 18.10±14.82, P> 0.05). The patients with liver disease also did not show any significant differences between pre and postprandial states (mean percentage of liver responding pre intake: 62.50±14.08, mean percentage of liver responding post intake: 72.98±10.59, P> 0.05). A sample response map for a healthy individual and a liver disease patient are shown in figure 5.3 for both pre and post intake sessions.

In the second analysis technique, the percentage difference between the means of the responsive pixels from the pre and post intake images was computed for each of the subjects along with the p-value from the t-test. Table 5.3 shows the percent change in liver response between these two states for healthy individuals (1-8) and patients suffering from chronic liver disease (9-11). P-values less than 0.05 indicate that the change was significant (unpaired student t-test).

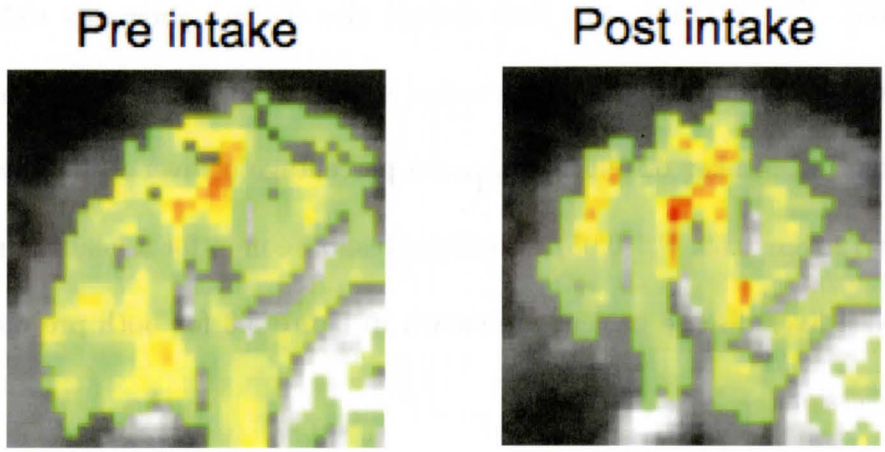

(a) Pre and postprandial response maps for a healthy individual.

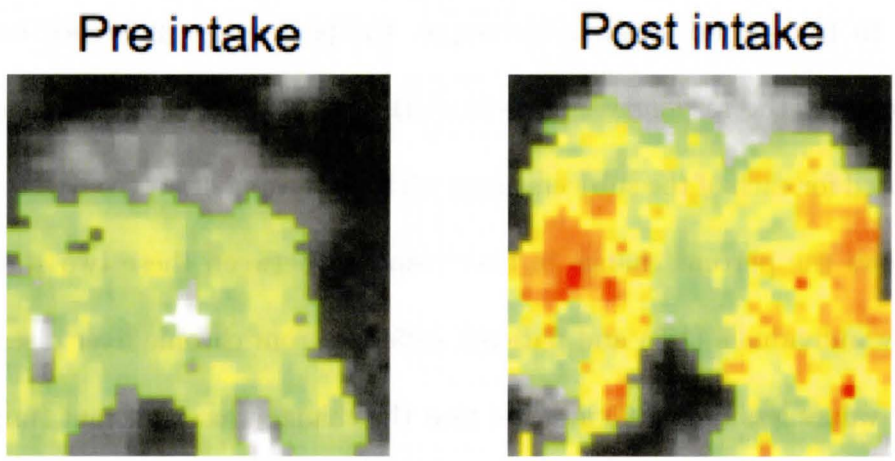

(b) Pre and postprandial response maps for a patient with chronic liver disease (in this case hepatitis-C)

Figure 5.3: The response maps for the pre and post intake sessions for one healthy subject and one patient with chronic liver disease. A hypothesis driven analysis method was used to obtain the response maps, here using gas cycling model 1.

Subject	% Difference in Liver Response Between Pre- and Postprandial States	P-value
1	1.29	0.55
2	-17.09	3.0×10^{-4}
3	-11.34	0.09
4	-98.56	7.7×10^{-6}
5	-65.43	0
6	-50.35	4.6×10^{-17}
7	-69.49	0
8	-88.16	2.6×10^{-20}
9	30.67	2.9×10^{-6}
10	109.51	0
11	-25.99	7.8×10^{-18}

Table 5.3: The percentage change in liver response between the pre and postprandial states for healthy subjects (1-8) and those with liver disease (9-11) using response maps from the hypothesis driven analysis and gas cycling model 1.

5.2.1.2 The Second Hyperoxia Model (Gas Cycling Model 2)

All subjects exhibited an increase in the BOLD signal intensity with the application of 100% O_2 (i.e. their response was as shown in figure 4.6). Figure 5.4 shows a sample BOLD time-series from one of the subjects.

The percent liver responding for healthy subjects was 78.79±10.59 (mean +/- standard deviation) in the pre intake session and 52.62±16.86 in the postprandial session. These differences were not statistically significant (P> 0.05, paired student t-test). The patients with chronic liver disease also did not show any significant differences between the two states (mean per-

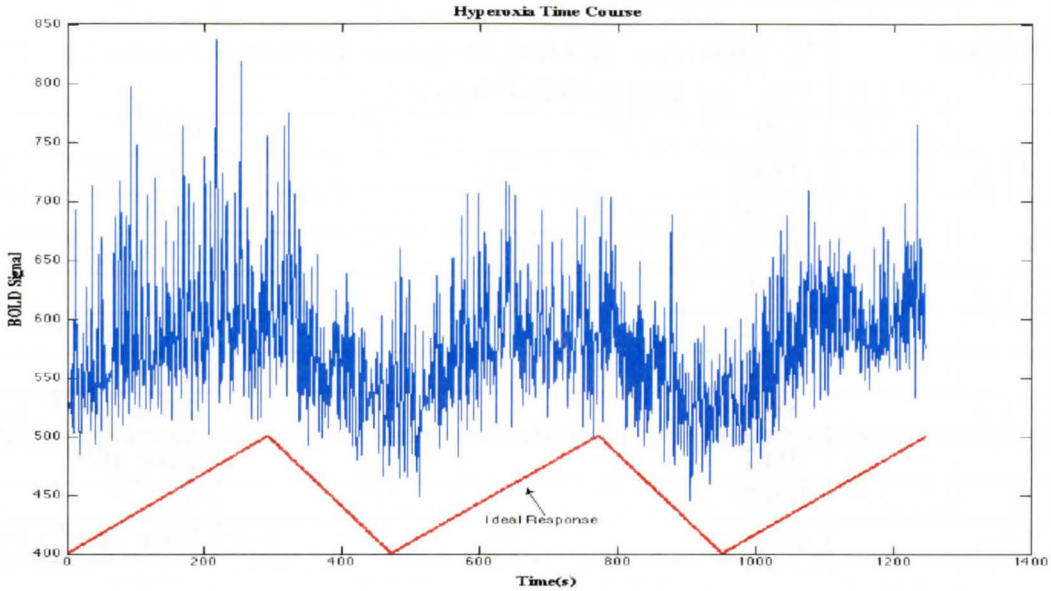

Figure 5.4: A sample time-series from one of the subjects with the modified set-up.

centage of liver responding pre intake: 49.20±26.04, mean percentage of liver responding post intake: 56.19±27.55, P> 0.05) Table 5.4 shows results for all participants. A sample response map for a healthy individual and a patient with hepatitis-C liver disease are shown in figure 5.5 for both pre and post intake sessions using hypothesis driven analysis.

Following GLM analysis a second analysis step was done where percent difference between means of responsive pixels, from pre and post intake images, was computed for each subject. Table 5.5 shows results for the healthy

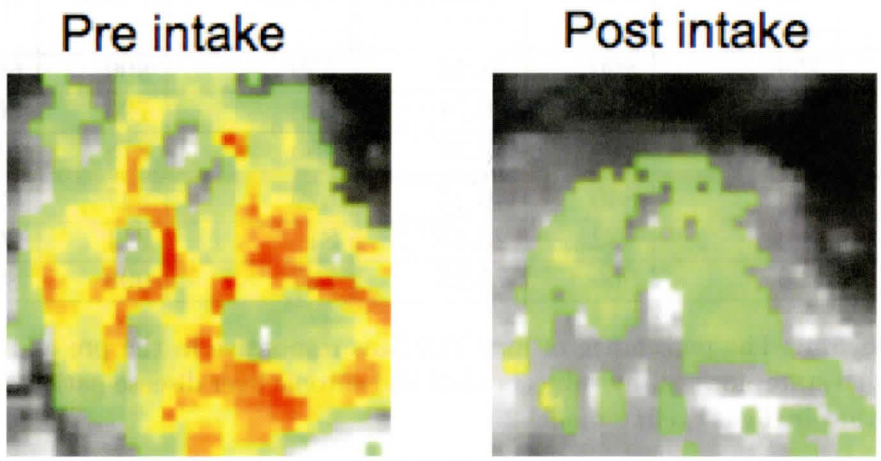

(a) Pre and postprandial response maps for a healthy individual.

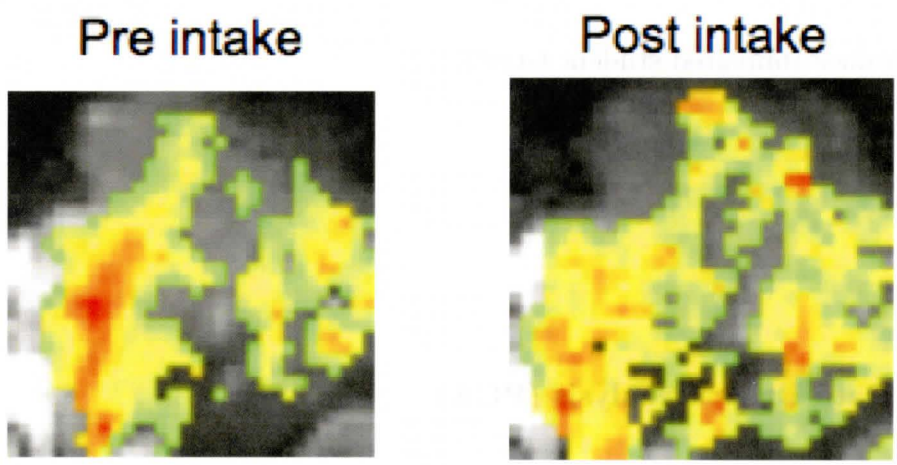

(b) Pre and postprandial response maps for a patient with chronic liver disease.

Figure 5.5: The response maps for the pre and post intake sessions for one healthy subject and one patient with chronic liver disease. A hypothesis driven analysis was used to obtain the response maps, here using gas cycling model 2.

	Pre intake			Post intake		
Subject	Responsive Liver Pixels	Total Liver Pixels	% of Liver Responding	Responsive Liver Pixels	Total Liver Pixels	% of Liver Responding
1	759	860	88.26	559	800	69.87
2	763	945	80.74	288	796	36.18
3	582	864	67.36	455	878	51.82
4	416	845	49.23	529	847	62.46
5	100	432	23.15	81	311	26.05
6	726	965	75.23	727	908	80.07

Table 5.4: The percentage of liver that was responsive in the pre and post-prandial states for healthy subjects (1-3) and chronic liver disease patients (4-6) using inspired gas cycling model 2.

subjects (1-3) and patients suffering from chronic liver disease (4-6) along with the p-values (unpaired student t-test).

5.2.2 Data Driven Analysis (PCA)

5.2.2.1 The First Hyperoxia Model (Gas Cycling Model 1)

Using data driven analysis (local PCA), the response maps were only analyzed by finding the percentage difference between the response value of the pixels from the pre and post intake images. Table 5.6 shows the percent

Subject	% Difference in Liver Response Between Pre- and Postprandial States	P-value
1	-60.11	0
2	-80.49	0
3	-32.22	1.5×10^{-16}
4	27.59	9.1×10^{-7}
5	47.36	0.005
6	-20.76	2.9×10^{-11}

Table 5.5: Percent change in liver response between pre and postprandial states for healthy subjects (1-3) and those with chronic liver disease (4-6) using response maps from the hypothesis driven analysis (i.e. GLM) with gas cycling model 2.

change in liver response between these two states for healthy individuals (1-8) and patients suffering from liver disease (9-11). Again, p-values less than 0.05 indicate that the change was significant (unpaired student t-test). A sample response map for a healthy individual and a liver disease patient are shown in figure 5.6 for both pre and post intake sessions using data driven analysis.

5.2.2.2 The Second Hyperoxia Model (Gas Cycling Model 2)

Using the second hyperoxia model, response maps were analyzed by finding the percentage difference between the response value of the pixels from the pre and post intake images for the maps obtained using local PCA. Table 5.7 shows the calculated results for the healthy subjects (1-3) and the

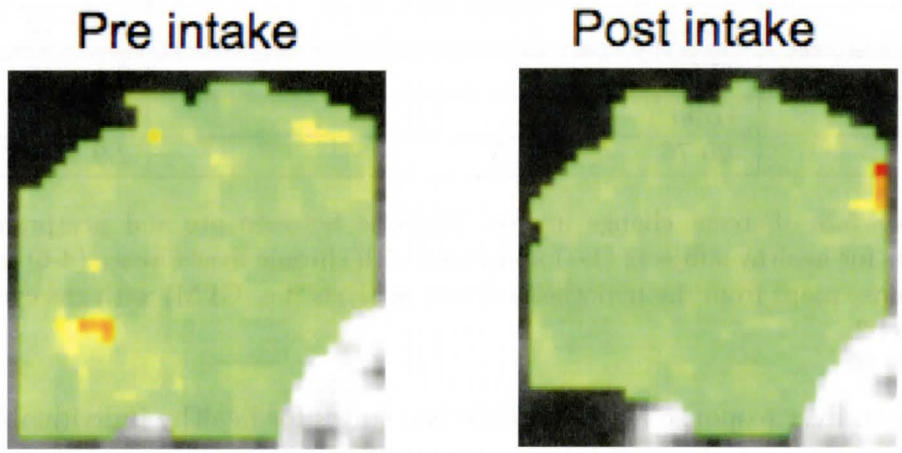

(a) Pre and postprandial response maps for a healthy individual.

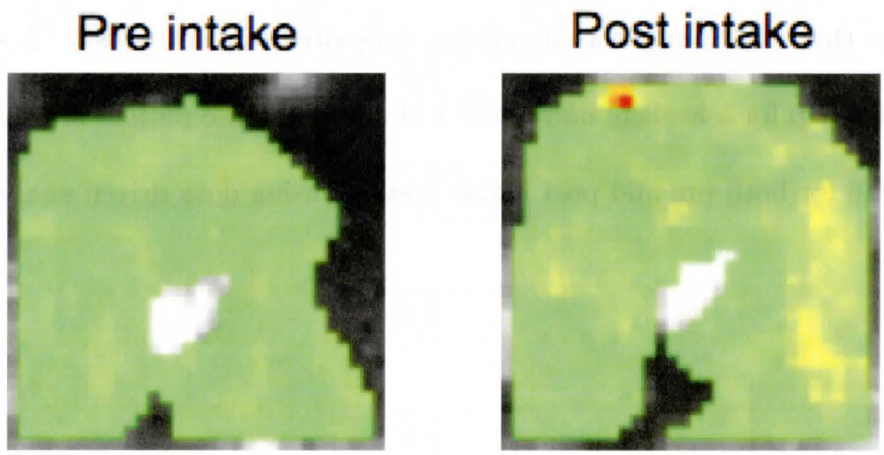

(b) Pre and postprandial response maps for a patient with liver disorder

Figure 5.6: The response maps for the pre and post intake sessions for one healthy subject and one patient with liver disorder Data driven analysis was used to obtain the response maps and gas cycling model 1

Subject	% Difference in Liver Response Between Pre- and Postprandial States	P-value
1	-6.09	0.17
2	-47.16	3.6×10^{-17}
3	3.16	0.10
4	-40.25	1.8×10^{-10}
5	-46.91	5.2×10^{-14}
6	13.37	0.9
7	-21.38	0.001
8	-29.91	1.1×10^{-7}
9	-2.01	0.39
10	122.63	3.2×10^{-40}
11	0.47	0.53

Table 5.6: The percentage change in liver response between the pre and postprandial states for healthy subjects (1-8) and those with liver disease (9-11) using response maps from the data driven analysis and with gas cycling model 1.

liver disease patients (4-6) along with the p-values obtained using the student unpaired t-test. A sample response map for a healthy individual and a liver disease patient are shown in figure 5.7 for both pre and post intake sessions using data driven analysis.

5.2.2.3 Timing of the Post Intake Session

One healthy subject was studied with the post intake session commencing immediately after meal intake and on another occasion where the data was

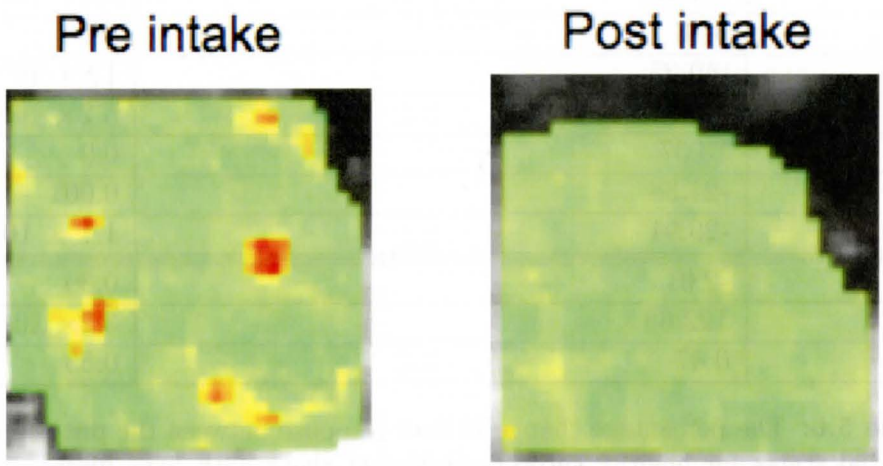

(a) Pre and postprandial response maps for a healthy subject.

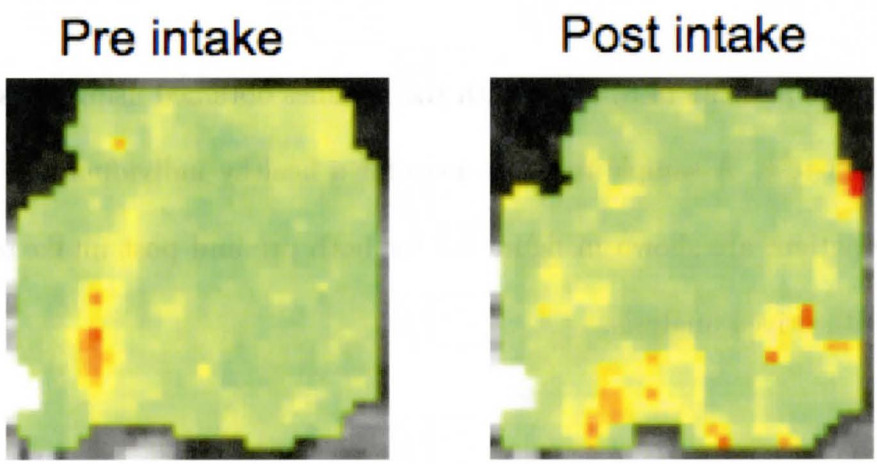

(b) Pre and postprandial response maps for a liver disease patient.

Figure 5.7: The response maps for the pre and post intake sessions for one healthy subject and one patient with liver disorder Data driven analysis was used to obtain the response maps and with gas cycling model 2.

Subject	% Difference in Liver Response Between Pre- and Postprandial States	P-value
1	-68.96	2.9×10^{-37}
2	-60.13	1.2×10^{-31}
3	-2.12	0.06
4	27.29	1.1×10^{-4}
5	50.57	0.001
6	9.93	0.9

Table 5.7: The percentage change in liver response between pre and postprandial states for healthy subjects (1-3) and those with liver disease (4-6) using response maps from the data driven analysis with gas cycling model 2.

Set-up	% Difference in Liver Response Between Pre- and Postprandial States	P-value
Session 2 commencing immediately following intake	-22.31	8.1×10^{-5}
Session 2 commencing 30 minutes following intake	-68.96	2.9×10^{-37}

Table 5.8: The percentage change in liver response between the pre and postprandial states for one healthy subject where the second session began either immediately following meal intake or 30 minutes postprandial.

collected thirty minutes post intake. Table 5.8 shows although the percent difference in response is similar, waiting 30 minutes produces 3 times greater BOLD percent change, with much higher degree of significance. Figure 5.8, shows the difference in response maps for pre and postprandial healthy liver comparing these timing differences.

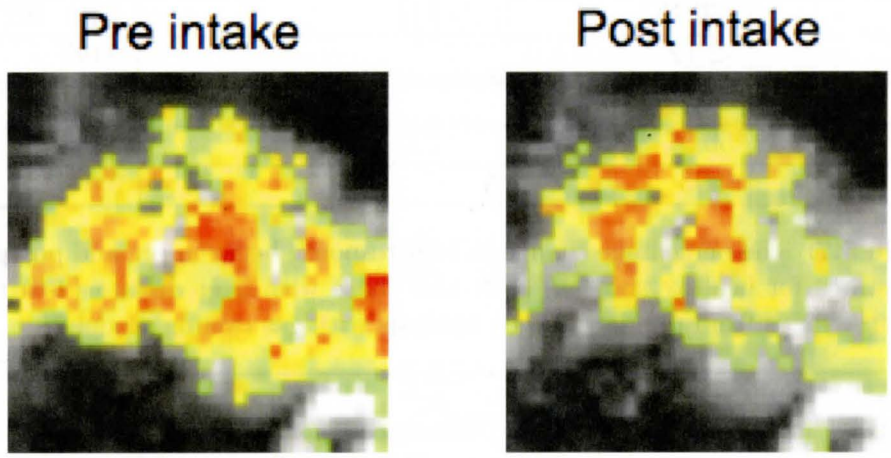

(a) Pre and postprandial response maps where session 2 commenced immediately following meal intake.

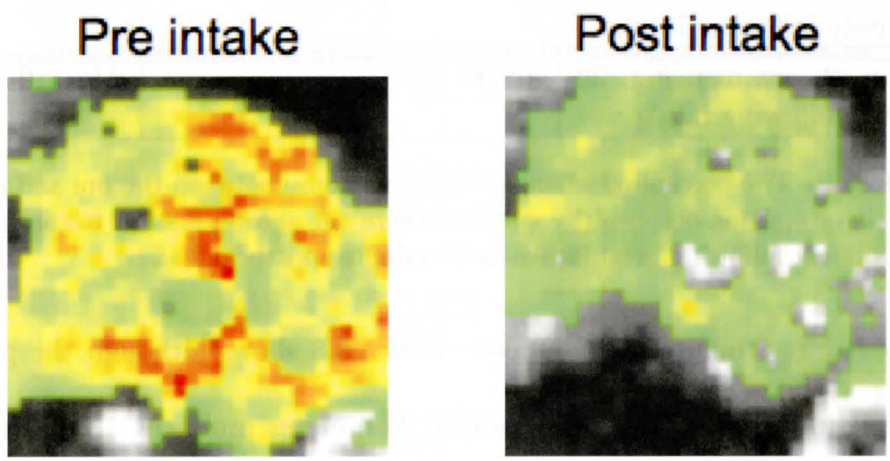

(b) Pre and postprandial response maps where session 2 commenced 30 minutes following meal intake.

Figure 5.8: The response maps for the pre and post intake sessions for one healthy subject where the second session began either immediately following meal intake (5.8(a)) or 30 minutes postprandial (5.8(b))

Chapter 6

Discussion

6.1 Blood Flow

Doppler sonography has been used by various research groups to evaluate the effects of food intake on hepatic circulation (Lafortune et al. (1993), Dauzat et al. (1994), Iwao et al. (1996), Salo et al. (1997)). All such studies confirmed that following the ingestion of a meal, hepatic portal blood flow increases. Iwao et al. (1996) monitored changes in hepatic portal blood flow at thirty minute intervals, up to 120 minutes after meal consumption and found that statistically significant changes were obtained at all measurement intervals. In addition, their work revealed that maximal postprandial changes resulted at thirty minutes following food intake. These findings were further confirmed in a study by Dauzat et al. (1994) who evaluated alterations in the volume of blood flowing through the main portal vein at fifteen, thirty, forty-five, and sixty minutes after the ingestion of two cans of Ensure. They reported increases in blood flow at all intervals and maximal postprandial

changes were seen at thirty minutes after intake, with a 79% increase at this interval in comparison to basal values (Dauzat et al. 1994).

In our study, hepatic portal vein blood flow was determined using phase contrast MR imaging. This technique had been previously used to evaluate blood flow (Pelc et al. (1992), Sadek et al. (1996), Hara et al. (1996)) and was shown to produce superior images of the hepatic portal vein (Hara et al. 1996). However, it had not been used to track haemodynamic changes in hepatic circulation that result from the ingestion of a meal, nor had it been employed to evaluate when such changes were maximal. Our findings showed that statistically significant increases in hepatic portal vein flow resulted from the intake of the standardized meal at all measurement intervals. Moreover, maximal postprandial changes were seen at thirty minutes after ingestion, with a 71% increase in comparison to the baseline flow. These findings were in agreement with the results of previous studies that were carried out using Doppler sonography (Dauzat et al. (1994), Iwao et al. (1996)).

We have demonstrated that phase contrast MR imaging can produce comparable results to those obtained using Doppler sonography when tracking postprandial changes over an interval. Although both MRI and Ultrasound are capable of non-invasively imaging blood flow in a vessel of choice, MRI provides some advantages over Duplex Doppler sonography when it comes to evaluating

portal vein blood flow, especially if a breath-held, 2D phase contrast sequence is used. This is because Duplex Doppler sonography measurements rely heavily on the placement of the angle of insonation (Paulson et al. (1997), Sadek et al. (1996)). Since it is difficult to consistently position the angle of insonation, large variation is seen when ultrasound is used to measure flow(Paulson et al. 1997). However, this issue is not a problem for MRI. Also, using a breath held sequence minimizes the motion of the portal vein and results in high quality images (Hara et al. 1996), allowing accurate detection of vessel edges and correct determination of flow values.

Based on blood flow results it was decided that in order to maximize pre-intake compared to postprandial BOLD signal contrast, images were to be collected at thirty-minutes after meal ingestion (i.e. the time to peak hepatic portal vein flow).

6.2 BOLD

One objective of this project was to optimize the current liver BOLD protocol experimental set-up and data analysis techniques. Some of the changes that were made to the set-up included asking the subject to drink the Ensure using a cup and straw (as opposed to having subjects ingest the drink while in the bore of the magnet from a tube connected to an Enema bag containing

the food contents, which the original set-up employed). This change made the study more subject-friendly as it eliminated anxieties that may have resulted from having the meal contents rapidly empty into the mouth, forcing rapid food ingestion during scanning. All healthy subjects and patients with chronic liver disorders who took part in the study were satisfied with the set-up and did not express any anxieties regarding meal ingestion since this intake method was one more natural. One draw back of this new set-up was that a person had to come into the room to supply the subject with the meal and had to hold the cup while the subject sipped the contents. However, the presence of a person in the MR room was necessary anyway to manipulate the gases during the remainder of the study, so this was just a minor issue. Another change to the set-up was that instead of performing the second hyperoxia session immediately after food intake (which was done previously ((Fan 2006))), the post Ensure BOLD acquisition was performed thirty-minutes postprandial. This was done in hopes of maximizing liver parenchyma BOLD contrast as our HPV blood flow studies resulted in maximal flow thirty minutes after intake. Since the BOLD signal intensity is proportional to the ratio of oxyhemoglobin to deoxyhemoglobin, in order to maximize the difference in BOLD intensity between a basal state and a state that accompanies physiological changes due to meal intake, data collection was performed when there was maximal blood

flow due to food ingestion. The response maps in figure 5.8 reveal that in fact, a larger change between the pre and post intake states was evident on the response maps when the BOLD data was collected at the time to peak hepatic portal vein flow. The percentage change in liver response between the pre and postprandial states was found to be -22.31% and -68.96% when the second BOLD session began immediately following meal intake and 30 minutes postprandial, respectively.

Since negative responders were seen, modifying the gas cycling by reversing the order of when 100% O_2 and medical air were supplied was tested to see if this would eliminate those responders. Although none were found among the three healthy and the three diseased subjects recruited, this may be just due to the small sample size and not necessarily the fact that this was a better ordering of the gases. It should be noted that for both gas cycling experiments (Figures 4.1 and 4.2), the timing for the application of medical air and 100% O_2 did not seem to have an effect on the BOLD signal's recovery to baseline (Figures 5.2 and 5.4). As this part of the challenge lasted twenty-one minutes, future testing might focus on testing different gas cycle timings to determine whether decreasing the time of the challenge has an affect on the final results. If not, then shorter scan times can be implemented.

In terms of data analysis, a few changes were implemented compared to that previously done ((Fan 2006)). Originally, the percentage of the liver that was responsive was assumed to be a good measure of the viability of the liver. In this technique, the number of pixels that showed response to the applied stimulus was counted and then divided by the total number of liver pixels, giving a response percentage. However, this approach has a limitation in that it does not take into account the degree of response of each of the responsive pixels. For instance, two pixels might show response to an applied stimulus, however, one might weakly respond, while another might respond strongly. This important information is omitted when only the number of pixels (and not their actual response) is used in the calculation. Looking at any of the figures that represent the response maps for the pre and post intake sessions for either healthy or diseased subjects (Figure 5.3, Figure 5.6, Figure 5.5, Figure 5.7), it can be seen that there is in fact a change in the response of pixels and not just in the number of pixels that are responsive. Thus, although analysis of the data was carried out in this project by calculating the percentage of the liver that was responsive, this was only done as an extension of the previous work. Using this analysis method, no statistically significant changes were found between the pre and post intake sessions using gas cycling model 2 for healthy subjects (mean percentage of liver responding pre intake: 78.79±10.59, mean

percentage of liver responding post intake: 52.62±16.86, P> 0.05) or liver disease patients (mean percentage of liver responding pre intake: 49.20±26.04, mean percentage of liver responding post intake: 56.19±27.55, P> 0.05). In addition, using gas cycling model 1, only the positive-responding subjects showed differences between the states that were statistically significant (mean percentage of liver responding is 53.73±23.40 in the pre intake session and 38.14±20.57 in the postprandial session, P< 0.05). This was not the case for the negative-responders or the patients (for negative responders, mean percentage of liver responding pre intake: 28.28±20.12, mean percentage of liver responding post intake: 18.10±14.82, P> 0.05, for chronic liver disease patients, mean percentage of liver responding pre intake: 62.50±14.08, mean percentage of liver responding post intake: 72.98±10.59, P> 0.05).

To make use of the response values of each pixel, the response maps were analyzed using a method other than the percentage difference, which was previously employed. In this second approach, a t-test was performed between the means of the pre and post intake response maps for a given subject to determine if a differential effect of the meal on the response of the subject could be observed. The difference in the means of the response values between the two states (post intake - pre ingestion) was then calculated. This value was turned into a percent difference via normalizing with the pre intake value

and multiplying the resultant number by 100. Using this technique, with gas cycling model 1 and a hypothesis driven GLM analysis, most healthy subjects (6 of the 8) showed significant decrease in liver BOLD contrast following meal intake, while two healthy subjects did not show any significant difference between the two states (Table 5.3). In addition, two of the patients showed statistically significant BOLD contrast increases following intake, while a significant decrease was observed in one patient (Table 5.3). Using the second gas cycling model and a hypothesis driven GLM analysis, all healthy subjects showed significant decreases in BOLD contrast with meal intake, while a significant increase was observed in two of the three patients (Table 5.5). A significant decrease in BOLD contrast was observed in the third patient, similar to the results of the healthy subjects. With such variation between subjects and patients, the GLM hypothesis driven approach was not able to differentiate between healthy and diseased, with either model of cycling inspired gases.

Since the liver has a dual blood supply, it was hypothesized that using a model-free approach may be more accurate when it comes to evaluating changes that accompany an applied stimulus. Due to the complex blood supply, it is quite likely there are complex delays that manifest as temporal phase shifts in the BOLD signal, thus giving what appears to be opposite of our suggested ideal wave. Whatever the source of data shifts, it is quite clear that

GLM based approaches are not appropriate for liver BOLD analysis. Using data driven analysis, specifically the PCA technique, no prior knowledge about the expected response of the liver had to be made. The only assumption was that two states existed, one for the application of 100% O_2 and one for the application of medical air. When this technique was used, it eliminated the issue of having negative responders, visible because their response was the opposite or out of phase with that predicted by the model. When a model-free approach was applied, the response was based on changes between the two states (hyperoxia and normoxia), and not on some a priori assumed correlation between the model and the BOLD data. This was a major improvement in liver BOLD analysis. One problem with having negative and positive responses is that if an individual exhibits some negative and some positive responding pixels, it becomes difficult to try and decide if this individual should be classified as a negative responder or a positive responder. Figure 6.1(a) shows the negatively responding pixels for one of the subjects. The positively responding pixels for the same subject are shown in Figure 6.1(b). Note that this subject was classified as a negative responder because the response maps showed more negative than positive pixels. However, this individual could have also been classified as a positive responder since the response map does show some positively responding pixels. Thus, this issue can be avoided by using a technique

that only relies on detecting differences between the two states and not on the correlation between the response and a predicted model. Another limitation that was evident when using the model based GLM approach is that certain pixels that were seen to show response were not detected (Figure 6.2). This was likely because although they did show changes between the two states, these changes did not match those predicted by the model and thus, they were not considered to be responsive.

Based on the presented issues thus far, it can be said that in order to optimize the technique used to analyze the data collected during the liver challenges we used, the response values of each pixel, and not just the number of pixels, needs to be taken into consideration. In addition, a model-free approach (e.g. PCA) is desired, since trying to appropriately model liver BOLD signal is not possible with a simple GLM approach. This is likely due to the complex blood supply to the liver. Using PCA, the response values of the pixels, and the original cycling of gases, most healthy subjects (five out of eight) showed significant decreased liver BOLD contrast following meal intake, while three healthy subjects did not show significant difference between the two states (Table 5.6). For patients, one showed significant increase in BOLD contrast, while two did not show significant changes (Table 5.6). Using our second gas cycling model, two of the healthy subjects showed significantly

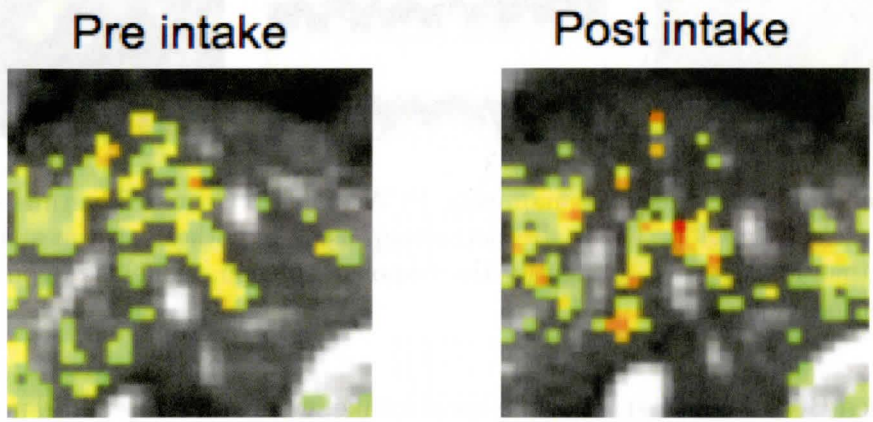

(a) Pre and postprandial response maps for a subject who was considered to be a negative responder The negative responding pixels are shown in both states.

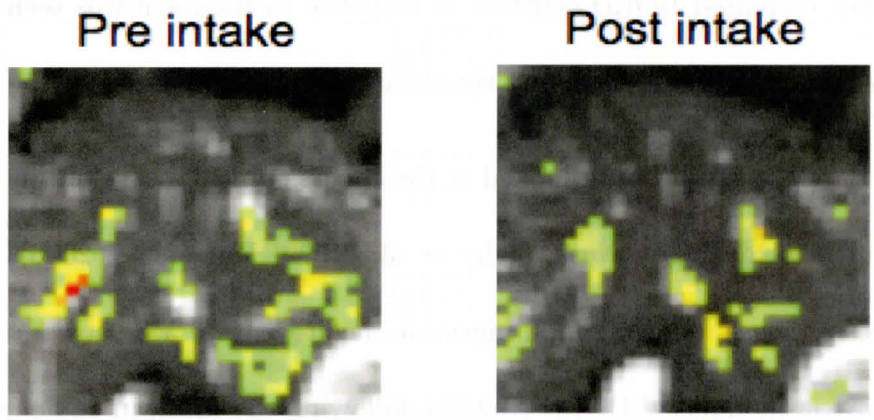

(b) Pre and postprandial response maps for the same subject showing the positive responding pixels.

Figure 6.1: The response maps for the pre and post intake sessions for one healthy subject using a negative ideal wave response(6.1(b)) and a positive ideal wave response (6.1(a)) in the hypothesis driven analysis.

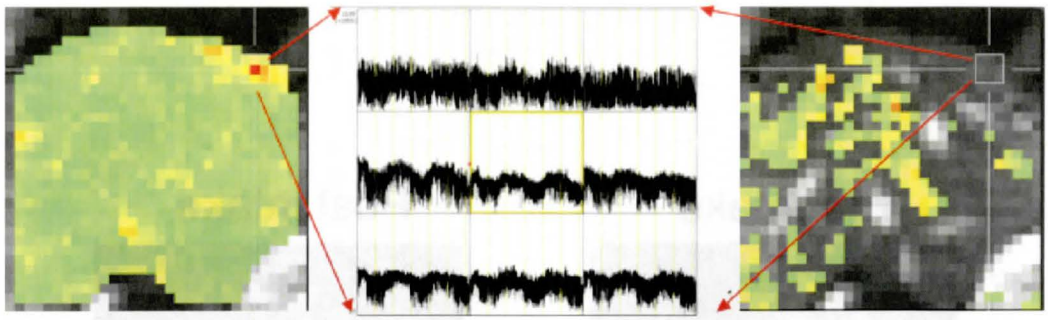

Figure 6.2: Left. Response map using PCA analysis. Center· The time-series of the selected region. Right. Response map using hypothesis driven analysis. Note that PCA is able to identify the responsive region, while the hypothesis driven technique is not.

decreased BOLD contrast following meal intake, while one subject did not show any significant difference between the two states (Table 5.7) For patients, significant increased BOLD contrast in response to the meal was seen in two cases, while one did not show any significant change (Table 5.7)

Based on studies that looked at the effects of meal intake on the BOLD signal in healthy livers (Noseworthy et al. 1999)(Fan et al. 2006), it was hypothesized that following food ingestion, healthy livers will show a decrease in hyperoxia-modulated BOLD contrast following the meal, in comparison to the pre intake response. Diseased livers, on the other hand, were postulated to respond differently; either showing an increase in response to the meal, or no significant change due to food ingestion. Using the first gas cycling approach, results from hypothesis driven analysis showed two subjects and one patient who did not fit these predictions. With PCA, all patients fit the

expected predictions, but three healthy individuals did not. With the second gas cycling method, one patient did not fit the expected predictions, while PCA showed all patients to fit the expectations and only one healthy subject did not.

When combining all results (eleven healthy subjects and six disease patients), the model-free PCA approach was able to detect all of the diseased livers, while missing four of the healthy subjects. The model-based GLM technique, on the other hand, did not detect two of the patients and two of the healthy subjects. Thus, if this liver challenge is to be used as a screening tool, then a model-free data analysis approach is more appropriate as it minimizes the chances of reporting false-negative results (i.e. has higher specificity). Although more false positives were detected with this method, these can easily be sorted out using more tests. In fact, as a screening tool, it is desirable to try and limit the false negative responses since concluding that a disease is not present when a person does actually suffer from it has detrimental effects. In addition, it should be noted that using a different model-free approach (such as partial least squares (PLS) instead of principle component analysis) may minimize the number of false positives detected. This can be tested in future studies.

One of the limitations of the current study is that in order to track the motion of the liver, rigid registration was used. However, the liver does also get deformed as it moves. Thus, a non-rigid registration technique should be evaluated and used in the future (if possible). In addition, registration of the pre and post intake images should be carried out for each of the subjects. This will ensure that correct inferences can be made about the response maps obtained from the two sessions.

In conclusion, the BOLD MR imaging liver challenge that had been previously developed was optimized using hepatic portal vein blood flow results. In addition, as the liver has a complex dual blood supply, a model-free approach, such as PCA, was shown to provide more reliable results than GLM approaches when analyzing BOLD time-series data. The optimized liver challenge was tested on healthy individuals and patients with chronic liver disorders and the protocol is able to distinguish between these two classes. Although promising results were obtained, further studies are needed before implementing the technique as a screening tool.

Bibliography

Abbattista, T., F. Ridolfi, E. Ciabattoni, F. Marini, E. Bendia, E. Brunelli, and P. Busilacchi (2008). Diagnosis of liver cirrhosis by transit-time analysis at contrast-enhanced ultrasonography. *Radiol Med 113*, 860–874.

Abdullah, S. S., J. B. Pialat, M. Wiart, F. Dubeouf, J.-Y. Maburt, B. Bancel, A. Rode, C. Ducerf, J. Baulieux, and Y. Berthezene (2008). Characterization of hepatocellular carcinoma and colorectal liver metastasis by means of perfusion mri. *J. Magn. Reson. Imaging 28*, 390–395.

Anderson, A. H., D. M. Gash, and M. J. Avison (1999). Principal component analysis of the dynamic response measured by fmri: A generalized linear systems framework. *Magn. Reson. Imaging 17*, 795–815.

Bacon, B. R. and A. M. D. Bisceglie (2000). *Liver Disease: Diagnosis and Management.* Churchill Livingstone.

Caruso, G., B. Valentino, G. Salvaggio, E. F. Lipari, D. Lipari, G. Brancatelli, R. Lagalla, and A. E. Cardinale (2005). Ultrastructural biologic effects of sonography with pulse inversion and microbubble contrast in rabbit liver. *Journal of Clinical Ultrasound 33*, 106–111.

Chezmar, J. L., W. M. Rumancik, A. J. Megibow, D. H. Hulnick, R. C. Nelson, and M. E. Bernardino (1988). Liver and abdominal screening in patients with cancer: Ct versus mr imaging. *Radiology 168*, 43–47.

Choi, S. H., J. M. Lee, N. C. Yu, K.-S. Suh, J.-J. Jang, S. H. Kim, and B. I. Choi (2008). Hepatocellular carcinoma in liver transplantation candidates: Detection with gadobenate dimeglumine-enhanced mri. *AJR 191*, 529–536.

Dauzat, M., M. Lafortune, H. Patriquin, and G. Pomier-Layrargues (1994). Meal induced changes in hepatic and splanchnic circulation: a noninvasive doppler study in normal humans. *Eur J Appl Physiol Occup Physiol 68*, 373–380.

Fan, Z. (2006). Functional study of human liver using bold magnetic resonance imaging. Master's thesis, McMaster University.

Fan, Z., M. D. Noseworthy, and C. Boylan (2007). Functional liver imaging using inter-pixel cross correlation (ipcc): A brute force univariate approach. *Proc. Int. Soc. Magn. Reson. Med. (ISMRM) 15*, 2722.

Fan, Z., M. Sussman, J. Stainsby, and M. Noseworthy (2006). Bold mri signal analysis of activated human liver. *Proc Int Soc Magn Reson Med. 14*, 3249.

Foley, L. M., P. Picot, R. T. Thompson, M. J. Yau, and M. Brauer (2003). In vivo monitoring of hepatic oxygenation changes in chronically ethanol-treated rats by functional magnetic resonance imaging. *Mag. Reson. Med. 50*, 976–983.

Friedrich-Rust, M., M.-F. Ong, E. Herrmann, V. Dries, P. Samaras, S. Zeuzem, and C. Sarrazin (2007). Real-time elastography for noninvasive assessment of liver fibrosis in chronic viral hepatitis. *AJR 188*, 758–764.

Geladi, P. and H. Grahn (1996). *Multivariate Image Analysis.* John Wiley and Sons.

Geller, S. A. and L. M. Petrovic (2004). *Biopsy Interpretation of the Liver.* Lippincott Williams and Wilkins.

Hara, A. K., D. J. Burkart, C. D. Johnson, R. L. Ehman, and D. M. Ilstrup (1996). Abdominal phase-contrast mr angiography: Breath-hold versus non-breath-hold techniques. *J. Magn. Reson. Imaging 1*, 94–98.

Huettel, S. A., A. W. Song, and G. McCarthy (2004). *Functional Magnetic Resonance Imaging.* Sinauer Associates, Inc.

Iwao, T., A. Toyonaga, H. Shigemori, K. Oho, T. Saki, C. Tayama, H. Masumoto, M. Sato, and K. Tanikawa (1996). Hepatic artery hemodynamic

responsiveness to altered portal blood flow in normal and cirrhotic livers. *Radiology 200*, 793–798.

Kinkel, K., Y. Lu, M. Both, R. S. Warren, and R. F. Thoeni (2002). Detection of hepatic metastases from cancers of the gastrointestinal tract by using noninvasive imaging methods (us, ct, mr imaging, pet): A meta-analysis. *Radiology 224*, 748–756.

Lafortune, M., M. Dauzat, G. Pomier-Layrargues, D. Gianfelice, L. Lepanto, G. Breton, D. Marleau, M. Dagenais, and R. Lapointe (1993). Hepatic artery: Effect of a meal in healthy persons and transplant recipients. *Radiology 187*, 391–394.

Lai, S.-H. and M. Fang (1999). A novel local pca-based method for detecting activation in signals in fmri. *Magn. Reson. Imaging 17*, 827–836.

Meeks, R. G., S. D. Harrison, and R. J. Bull (1991). *Hepatotoxicology*. CRC Press.

Noseworthy, M., D. Bulte, and J. Alfonsi (2003). Bold magnetic resonance imaging of skeletal muscle. *Semin Musculoskel Radiol 7*, 307–315.

Noseworthy, M., J. Kim, J. Stainsby, and G. Wright (1999). Biexponential t_2 analysis of human liver in the fasted and postprandial states: potential

for monitoring tissue microcirculatory changes. *Proc Int Soc Magn Reson Med. 7*, 2148.

Noseworthy, M. D., M. A. Haider, M. S. Sussman, and G. A. Wright (2007). Free-breathing motion compensation using template matching: a technique allowing for tracer kinetic modeling of liver metastases. *J Comput Assist Tomogr 31*, 193–197.

Ogawa, S., T. Lee, A. Nayak, and P. Glynn (1990). Oxygenation-sensitive contrast in magnetic resonance image of rodent brain at high magnetic fields. *Mag. Reson. Med. 14*, 68–78.

Oliva, M. R. and S. Saini (2002). Liver cancer imaging: Role of ct, mri, us and pet. *Cancer Imaging 4*, 542–546.

Oliveri, F., B. Coco, P. Ciccorossi, P. Colombatto, V. Romangnoi, B. Cherubini, F. Bonino, and M. R. Brunetto (2008). Liver stiffness in the hepatitis b virus carrier: A non-invasive marker of liver disease influenced by the pattern of transaminases. *World J Gastroenterol 14*, 6154–6162.

Paulson, E. K., M. A. Kliewer, M. G. Frederick, M. T. Keogan, D. M. DeLong, and R. C. Nelson (1997). Doppler us measurement of portal venous flow: Variability in healthy fasting volunteers. *Radiology 202*, 721–724.

Pelc, L. R., N. J. Pelc, S. C. Rayhill, L. J. Castro, G. H. Glover, R. J. Herfkens, D. C. Miller, and R. B. Jeffrey (1992). Arterial and venous blood flow: Noninvasive quantitation with mr imaging. *Radiology 185*, 809–812.

Sadek, A. G., F. B. Mohammed, E. K. Outwater, S. S. ElEssawy, and D. G. Mitchell (1996). Respiratory and postprandial changes in portal flow rate: Assessment by phase contrast mr imaging. *J. Magn. Reson. Imaging 1*, 90–93.

Salo, S., A. Alanen, M. Komu, T. Kallio, and S. Bondestam (1997). Effect of fasting and food intake on magnetization transfer of human liver tissue. *Magn. Reson. Imaging 15*, 47–50.

Semple, S. I., F. Wallis, P. Haggarty, D. Abramovich, J. A. Ross, T. W. Redpath, and F. J. Gilbert (2001). The measurement of fetal liver t_2^* in utero before and after maternal oxygen breathing: progress towards a non-invasive measurement of fetal oxygenation and placental function. *Magn. Reson. Imaging 19*, 921–928.

Sherlock, S. and J. Dooley (2002). *Diseases of the Liver and Biliary System* (Eleventh ed.). Blackwell Publishing.

Shier, D., J. Butler, and R. Lewis (2006). *Hole's Essentials of Human Anatomy and Physiology* (Ninth ed.). McGraw Hill.

Shuter, B., P. Tofts, and J. Pope (1995). The effects of sacrifice on image signal, t_1, t_2 and t_2^* in liver, kidney, and brain of the wistar rat. *Magn. Reson. Imaging 13*, 563–574.

Suma, H. N. and S. Murali (2007). Principal component analysis for analysis and classification of fmri activation maps. *International Journal of Computer Science and Network Security 7*, 235–242.

Sussman, M. S. and G. A. Wright (2003). Factors affecting the correlation coefficient template matching algorithm with application to real-time 2-d coronary artery mr imaging. *IEEE Trans Med Imag 22*, 206–216.

Talos, I.-F., A. Z. Mian, K. H. Zou, L. Hsu, D. Goldberg-Zimring, S. Haker, J. G. Bhagwat, and R. V. Mulkern (2006). Magnetic resonance and the human brain: anatomy, function and metabolism. *Cell. Mol. Life Sci. 63*, 1106–1124.

Theodoridis, S. and K. Koutroumbas (2003). *Pattern Recognition.* Elsevier Academic Press.

Appendix A

Matlab Code to Create a Registered BOLD Data Set

```
%This file corrects the motion in the BOLD time-series and outputs
% a registered .nii image set
%It uses the displacement data from "Motion Track"



% Input the dicom BOLD images that are to be registered
ser = 'Ser1/';                          % specify series #
exam = 'E1234S1I';                      % specify exam #
ext = '.MR.dcm';
for i = 1 : 1248
    num_str = num2str(i);
    filename = strcat(ser,exam,num_str,ext);
    A(:,:,i) = dicomread(filename);
end

%generate a new matrix to store the registered data
R = zeros(1,32,32,1248);

%Put the initial displacement & size of the template
posi = [10 7];
size = 32;

%load in the .txt file containing the location of the template
% that is generated using motion track program
disp = dlmread('1234_pre.txt');
```

```
%convert the inputed mm values into units of pixel
disp = disp(:,1:2)./4.375;


% Extract the template from the inputed time series
for i = 1 : 1248
    R(1,:,:,i) = imcrop(A(:,:,i),[disp(i,1)+10 disp(i,2)+7 31 31]);
end


% Create and save a .nii file (to be used in FSL)
nii = make_nii(R, [8 4.375 4.375]);
save_nii(nii,'registerd_pre.nii');
```

Appendix B

Matlab Code to Calculate the % of Liver that is Responsive

```
%This file calculates the percentage of the liver that is responsive


stat=load_nii('glm_pre.nii');      % load in liver response map
mask=load_nii('mask_pre.nii');     % load contoured liver

r=stat.img;                        %read the 32*32 response map


%find and display the number of responsive pixels
[row,col,v]=find(r);
num_of_responsive_pix=size(v)


m=mask.img;                         %read the contoured liver data

%find and display the total number of liver pixels
[row1,col1,v1]= find(m);
num_of_liver_pix=size(v1)

%find and display the % of the liver that's responsive
per_respon=100*(num_of_responsive_pix/num_of_liver_pix)
```

Appendix C

Matlab Code to Perform a T-test on the Extracted Liver Data

```
%This file loads in the liver response maps along with the
%liver masks and performs an unpaired t-test on the data


%load in the response map (.nii file) for the pre-intake data
%generated using hypeothsis driven analysis

stat1=load_nii('glm_pre.nii');


%load in the response map (.nii file) for the pre-intake data
%generated using data driven analysis
pca1=load_nii('pca_pre.nii')


%load in the mask liver data (.nii file) for pre-intake session
mask1=load_nii('mask_pre.nii');


%load in the response map (.nii file) for the post-intake data
%generated using hypothesis driven analysis
stat2=load_nii('glm_post.nii');

%load in the response map (.nii file) for the post-intake data
%generated using data driven analysis
pca2=load_nii('pca_post.nii');


%load in the mask liver data (.nii file) for post-intake session
mask2=load_nii('mask_post.nii');
```

```
%extract the only the liver data from the pre-intake response map
%genertated using hypothesis driven analysis
b1=pca1.img(mask1.img==1);

%extract the only the liver data from the post-intake response map
%genertated using hypothesis driven analysis
b2=pca2.img(mask2.img==1);

%extract the only the liver data from the pre-intake response map
%genertated using data driven analysis
c1=stat1.img(mask1.img == 1);

%extract the only the liver data from the post-intake response map
%genertated using data driven analysis
c2=stat2.img(mask2.img ==1);


%perform an unpaired ttest on extracted liver data(hypotheis drive)
[h_glm,p_glm]=ttest2(c2,c1,0.05,'left','unequal')


%find the percent difference between the means of the pre and post
%intake data (hypothesis driven)
glm_per= 100*((mean(c2)-mean(c1))/mean(c1))


%perform an unpaired ttest on the extracted liver data (data drive)
[h_pca,p_pca]=ttest2(b2,b1,0.05,'left','unequal')


%find the percent difference between the means of the pre and post
%intake data (data driven)
pca_per= 100*((mean(b2)-mean(b1))/mean(b1))
```